8 Devolatilization

8.1 Introduction, 409
8.2 Devolatilization Equipment, 411
8.3 Devolatilization Mechanisms, 413
8.4 Thermodynamic Considerations of Devolatilization, 416
8.5 Diffusivity of Low Molecular Weight Components in Molten Polymers, 420
8.6 Boiling Phenomena: Nucleation, 422
8.7 Boiling–Foaming Mechanisms of Polymeric Melts, 424
8.8 Ultrasound-enhanced Devolatilization, 427
8.9 Bubble Growth, 428
8.10 Bubble Dynamics and Mass Transfer in Shear Flow, 430
8.11 Scanning Electron Microscopy Studies of Polymer Melt Devolatilization, 433

8.1 INTRODUCTION

In the manufacturing process of most polymers, there is a need to separate and remove undesirable, residual volatile components such as solvents, monomers, and other low molecular weight components from the polymeric material. These volatiles are removed in one or more postreactor operations in order to recover the solvent and monomer, impart the polymer with the desired physical properties, meet environmental requirements, and eliminate residual odors and taste. In condensation polymerization, of course, the removal of volatiles is essential to drive the polymerization reaction and reach high molecular weights. Moreover, removal of volatiles, moisture and entrapped air is also essential for many types of down-stream compounding and processing equipment.

The elementary step of *devolatilization*, discussed in this chapter, refers to the removal of relatively low concentrations of volatiles of the order of 1% or less. Much of the research, which elucidated the devolatilization step, took place over the past two decades. Joseph A. Biesenberger, one of the pioneers of devolatilization research, published the first review on the subject in 1983 (1), and more recently, Ramon J. Albalak edited a volume devoted to this subject in 1996 (2).

Devolatilization is a mass transport operation. The molecules of the volatile components dissolved in the matrix of the polymeric melt must diffuse to liquid–vapor interfaces, and then be removed and collected. All devolatilization processes, irrespective of the complexity of the equipment in which they take place, are represented schematically by Fig. 8.1.

Principles of Polymer Processing, Second Edition, by Zehev Tadmor and Costas G. Gogos.

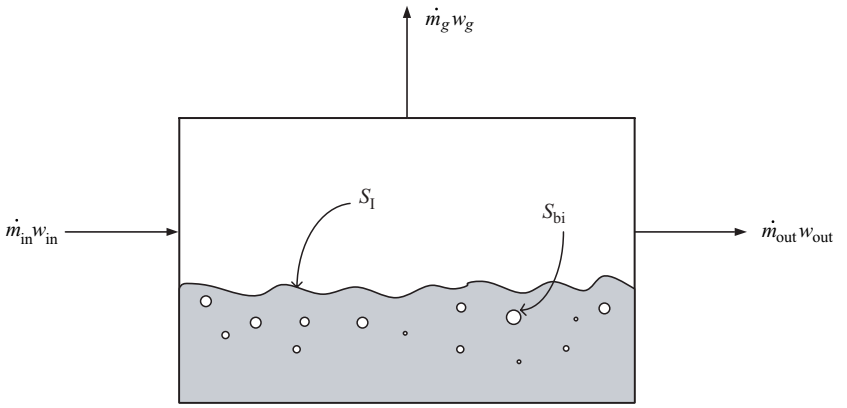

Fig. 8.1 Schematic representation of the devolatilization process. The hatched area represents the polymer melt being devolatilized, which is almost always subject to laminar flow. The bubbles shown are created by the boiling mechanism and by entrapped vapors dragged into the flowing/circulating melt by moving surfaces.

Under steady state operating conditions the macroscopic mass balance of the volatile component (Eq. 2.4-1) is given by

$$w_{\text{in}}\dot{m}_{\text{in}} - w_{\text{out}}\dot{m}_{\text{out}} - w_g\dot{m}_g = 0 \tag{8.1-1}$$

where $\dot{m}$ represents mass flow rate and w represents mass fraction of the volatile component. It is convenient to express the mass flow rate of the evaporating volatile component $w_g\dot{m}_g$ in terms of interface transport flux (1), that is, flow rate per unit area of the volatile component normal to the interfacial

$$w_g\dot{m}_g = k_m S_m \tag{8.1-2}$$

where k_m is a mass transfer coefficient and S_m is the total interfacial area given by

$$S_m = S_I + \sum_{i=1}^{N} S_{bi} \tag{8.1-3}$$

where S_I is the interfacial area of the melt surface and S_{bi} is the interfacial area of bubble i.

The objective is to reduce volatiles to below 50–100-ppm levels. In most devolatilization equipment, the solution is exposed to a vacuum, the level of which sets the thermodynamic upper limit of separation. The vacuum is generally high enough to superheat the solution and foam it. Foaming is essentially a boiling mechanism. In this case, the mechanism involves a series of steps: creation of a vapor phase by nucleation, bubble growth, bubble coalescence and breakup, and bubble rupture. At a very low concentration of volatiles, foaming may not take place, and removal of volatiles would proceed via a diffusion-controlled mechanism to a liquid–vapor macroscopic interface enhanced by laminar flow-induced repeated surface renewals, which can also cause entrapment of vapor bubbles.

Alternatively, a third, low boiling-point additive such as water or inert gas can be added to strip the residual volatiles, which (a) provides more mass transfer area, (b) reduces diffusion distance for the molecules that we wish to remove, (c) increases the driving force for the separation because of the lower concentration of the volatile in the bubbles, and (d) the vaporization of the stripping agent offsets some of the heat generated by viscous dissipation. Of course, after separation we have to deal with a dilute mixture of the volatile in the stripping agent, which may need to be separated for recovery and/or environmental reasons.

In this chapter, subsequent to an introduction to devolatilization equipment, we review the thermodynamics of polymer solution equilibrium, which determines the *maximum* amount of volatiles that can be separated under a given set of processing conditions; the phenomena associated with diffusion and diffusivity of small molecules in polymeric melts, which affects the rate of mass transfer; the phenomena and mechanisms involving devolatilization and their modeling and the detailed and complex morphologies within the growing bubbles created during devolatilization of melts.

8.2 DEVOLATILIZATION EQUIPMENT

As noted earlier, the polymeric melt systems in devolatilization have very low volatile concentration and therefore very high viscosities. Consequently their handling normally requires equipment with rotating elements similar or identical to polymer processing machinery such as single and twin screw extruders (SSEs, TSEs). These extruders are equipped with "venting ports," which expose the molten polymer to low absolute pressure levels, superheating the polymer–volatile mixture, and thus enabling the removal of the volatiles.

In industrial practice, high production postreactor streams, as well as compounding and reactive processing operations, need to be devolatilized. The devolatilization process significantly affects the manufacturing cost and is critical to the quality of the product. The equipment is complex and costly and also involves the recovery of the volatiles. Todd et al. (3) and Mehta (4) reviewed, in some detail, the commercial equipment used for devolatilization, which we briefly summarize later in this Section.

Dilute polymer solutions containing relatively large amounts of volatiles are devolatilized in ordinary, relatively low-cost, single or multiple stage *flash tanks*. The flash tank is fed via a preheater that superheats the solution. The vapors of the foaming–boiling solution are removed at the top of the tank by a vapor takeoff system, and the concentrated solution is removed at the bottom via a gear pump.

As viscosity increases with decreasing volatile content, the flash tank becomes inefficient as bubbles are entrapped and redissolved upon discharge. The *falling-strand devolatilizer*, shown schematically in Fig. 8.2, was developed to answer this problem, and represents an improvement over the ordinary flash tank. Here the polymer solution is pumped at high superheat into thin strands that fall gravitationally into the vacuum tank. Free of hydrostatic or shear-induced pressure fields, the bubbles nucleate, grow, coalesce, and rupture so that the volatiles are released before they get trapped in the melt of the cachepot.

As volatile levels drop further, yielding very concentrated polymer solutions, the viscosity increases to a level that requires *rotary equipment* for forward pumping of the solution, which imparts surface renewal and often entraps vapor bubbles, for improved mass and heat transfer as well. There is a wide variety of rotary equipment available, from advanced *ribbon* devolatilizers, *vertical-cone* devolatilizers, and *disk-ring* devolatilizers for moderately viscous solutions, to *single* and *twin screw* devolatilizers and *thin-film*

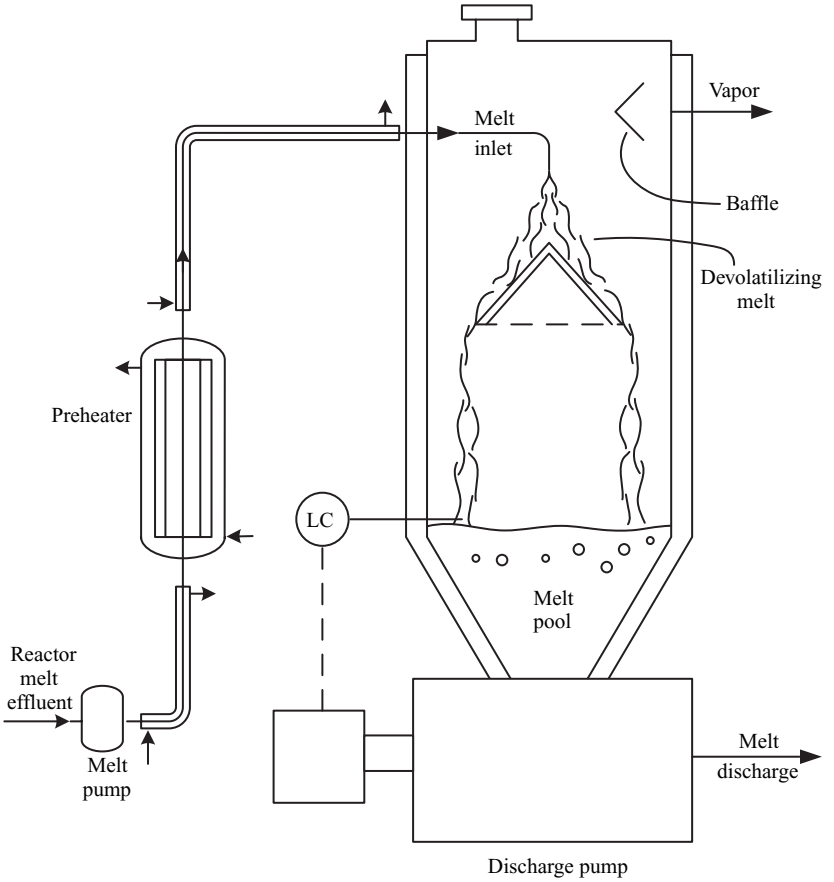

Fig. 8.2 A schematic view of a falling-strand devolatilizer.

devolatilizers for very high-viscosity solutions. Figure 8.3 shows a large, two-shaft reactor devolatilizer, and Fig. 8.4 shows a wiped thin-film evaporator.

In the case of devolatilization, industrial practice preceded theory, and the rich variety of equipment used in industry was developed without any thorough understanding of the molecular mechanisms by which devolatilization takes place. This, of course, is not an uncharacteristic phenomenon in technology, where practice often anticipates theory by providing "satisficing" design solutions.[1] These in turn become entrenched and reproduced in industry, even though there may perhaps be other better or even optimal and easily scalable design solutions.

1. The term *satisficing* was coined by the Nobel Prize–winning economist Herbert Simon, who suggested that in engineering (and management) as a *matter of principle* one should not look for an optimal solution, but only an adequate or *satisfactory* solution, since identifying the former may be a wasteful and time-consuming process with marginal added gain. Simon conveys a profound point regarding design and practice; however, this should not discourage us from the pursuit of theoretical understanding. The latter not only enhances our knowledge and may provide numerous other, possibly better, design solutions which, being theoretically driven, are more adaptable to industrial scale-up, but also enhances our understanding of current practices.

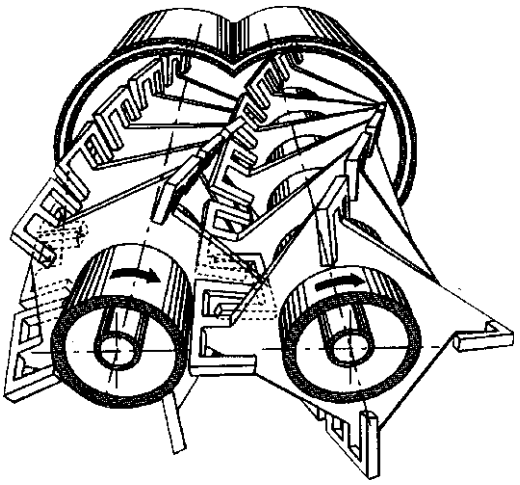

Fig. 8.3 Schematic representation of the List twin shaft co-rotating continuous mechanical and thermal processor. [Courtesy of the List Corporation.]

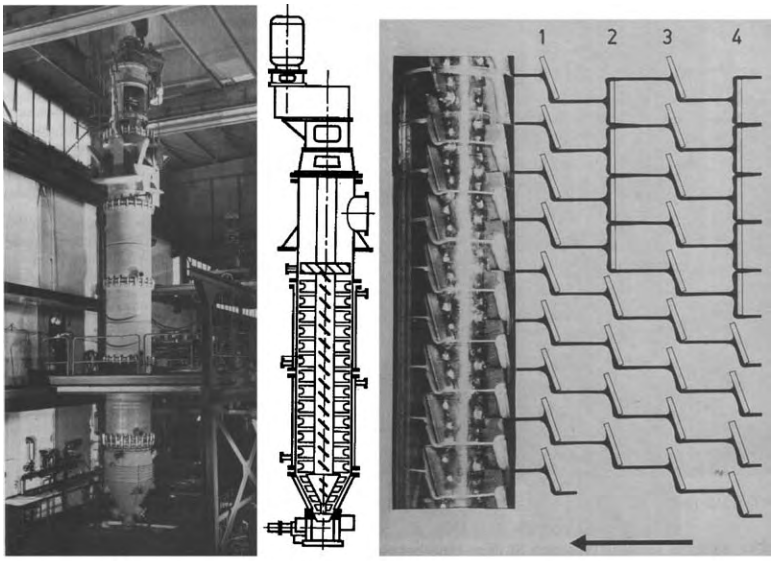

Fig. 8.4 Luwa Corporation Filmtruder (a) Filmtruder HS-1800. (b) Schematic representation of the Filmtruder. (c) Schematic representation of the falling- and wiped-film in the Filmtruder. [Courtesy Luwa Corporation.]

8.3 DEVOLATILIZATION MECHANISMS

Devolatilization of concentrated solution may start with an above atmospheric flash separation. This way the solvent and unreacted monomer can be easily and directly recycled. However, downstream all devolatilization equipment is operated under reduced

pressure or vacuum. This creates the superheat needed for separation and also makes the collection and condensation of the volatiles rather straightforward. In 1980, Newman and Simon (5) were the first to model theoretically the foaming mechanism in falling-film evaporators. They assumed a swarm of bubbles that grow, coalesce, rupture, and vacate their vapor content into the vapor space.

The pioneering researchers of devolatilization did not recognize, however, that at low volatile content when rotary equipment is used, in most cases, devolatilization takes place via a foaming–boiling process, with the vacuum level determining the supersaturation needed for bubble nucleation and growth. Rather, they initially conceived a molecular diffusion–controlled mechanism. Thus Latinen (6), who in 1962 was among the first to propose a theoretical mathematical model for devolatilization in SSEs, suggested that the mass transfer rate is controlled by molecular diffusion in the thin film deposited by the screw flight on the barrel surface in the partially filled vented region of the extruder, as shown in Fig. 8.5. The thin film, as it emerges from under the flight, is uniform in concentration C. As soon as the film surface is exposed to the vapor phase, its surface concentration drops to C^*, which is the volatile concentration in the solution at equilibrium with the vapor phase. This creates, for a short time period of one rotation, a high initial concentration gradient in the film, leading to possibly high mass transfer rates. Then the film is mixed with the rest of the solution in the rolling pool, and a new film, at a somewhat lower concentration, is deposited on the barrel. Therefore, by periodic *renewal* of the film, termed *surface renewal*, an overall high rate of mass transfer can be expected. This rate depends on the frequency of screw rotation, N, because the surface is renewed over a period of time of $1/N$, and on the

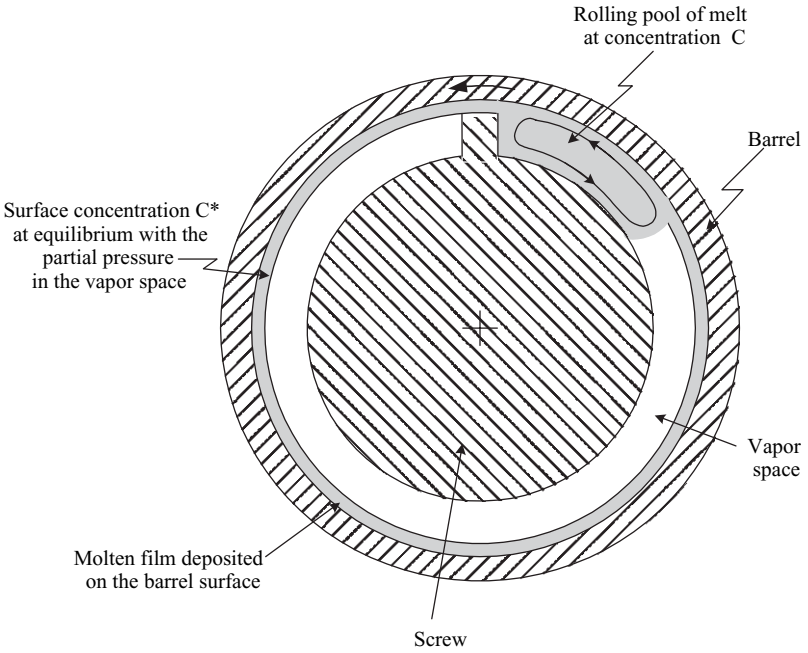

Fig. 8.5 Schematic representation of a screw section in the partially filled vented section of the extruder, according to Latinen (6).

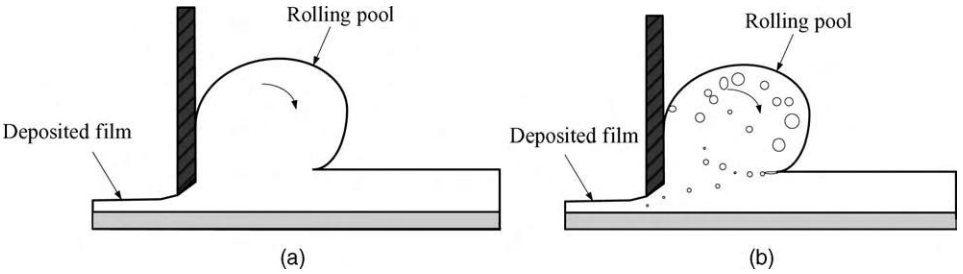

Fig. 8.6 (a) Schematic representation of the ''rolling pool deposited film'' mechanism. (b) The same mechanism, but with bubble formation and entrainment of vapor and noncondensable gas pockets, which act as nuclei in the boiling–foaming mechanism.

partial pressure of the volatile in the vapor space, which sets the value of C^*. According to this mechanism, the role of the vacuum level is limited only to setting the value of C^*. Of course, if the vapor phase would be swept with an inert gas, C^* could be reduced to practically zero without applying vacuum. The essence of this mechanism is shown in Fig. 8.6(a) consisting of a rolling pool and a deposited film exposed to low partial vapor pressure. However, we should note that pockets of vapor can become entrapped in the rolling pool, and provide the initial nucleation sites in wiped-film devolatilizers and extruders, as shown in Fig. 8.6(b).

Latinen (6) experimented with the separation of styrene from PS in a vented extruder. At the time, he did not have experimentally measured values of styrene diffusivity in molten PS and, therefore, from the experimentally measured separation he back-calculated the diffusivity. The values he attained were in the range of $10^{-9}\,m^2/s$ at 200°C. Today we know that these values are at least one order of magnitude too high. Latinen compared the results he got to diffusivities in low-viscosity systems and they appeared to him to be too high as well, leading him to suggest possible explanations, such as melt surface roughness and foaming. He subsequently rejected the latter as being unlikely for such viscous solutions. Several others tried to improve the Latinen model (7,8) by accounting for the contribution of the rolling pool to the separation by diffusion, but they too obtained unreasonably high values for the back-calculated diffusivities, indicating that this mechanism is unsatisfactory for explaining the devolatilization mechanism.

The definite proof that, even at such low levels of volatiles, the devolatilization mechanism in vented SSEs is a foaming–boiling one came from the work of Biesenberger and Kessidis (9) in 1982, Mehta et al. (10) in 1984, and Tukachinsky et al. (11) in 1994.

Biesenberger and Kessidis repeated Latinen's experiment in vented SSEs, but rather than applying vacuum over the vent, they flushed the vapor space with nitrogen. The separation they obtained was two orders of magnitude below the one obtained with vacuum and provided a reasonable match between the Latinen model and the real diffusivity values. Using the simple geometry of the co-rotating disk (CDP) processor, which enables accurate modeling as well as visual observation of the deposited film, Mehta et al. (10) concluded that, contrary to the surface renewal diffusion-controlled theory, the thinner the film, the poorer the separation efficiency. Moreover, they observed foaming on the deposited thin films on the disk surfaces. Finally, Tukachinsky et al. (11)

videotaped and observed the instantaneous foaming of 6000-ppm polystyrene–styrene solution in a 50-mm-diameter SSE upon the application of vacuum through an observation post in the barrel.

Yet in spite of all the evidence just presented, it is not impossible that at very low volatile levels the Latinen-type model may have some validity, but this likelihood appears to be small because foaming was observed at volatile concentrations as low as 50 ppm. Moreover, the likelihood further diminishes due to the fact that, as shown in Section 8.5, the diffusivity of small molecules in polymeric melts may drop by orders of magnitude, with dropping concentrations at these levels.

In the rolling pool-film configuration, however, normally nucleation, bubble growth and rupture take place primarily in the rolling pool. Nucleation is expected to be enhanced in the regions of stretching (negative pressure) in the rolling melt pool, and by entrainment of free, noncondensable gases at the pool–film junction where melt ''folding'' takes place by the moving solid surface, which creates microbubbles.

Bubble growth is enhanced by bubble deformation in the shear fields, and it was shown that the alternating pressure field existing in the rolling pool yields continuous bubble growth and bubble breakup. Bubble breakup in the shear fields increases the bubble population, and bubble rupture is induced in the bubbles close to the pool surface, where they release their content into the vacuum space. The total mass transfer surface significantly increases, because the sum total of bubble surfaces is much larger than that of the deposited film. For all these reasons, it is not surprising to find an increase in devolatilization efficiency with increasing speed of rotation.

In view of the foregoing discussion, and in order to better understand devolatilization in quantitative terms, in the following sections we will revisit elements of polymeric solution thermodynamics, briefly discuss diffusivity of small molecules in polymeric melts, review nucleation, bubble growth, bubble breakup, and bubble rupture theories, and elucidate them if possible in the shear-flow fields that occur in rotating-type devolatilizers. The chapter concludes with a discussion of experimental microscopic observations designed to ''look'' into the actual mechanisms taking place in boiling–foaming solutions, which led to surprising and unexpected results, and some suggestions for their theoretical formulation.

8.4 THERMODYNAMIC CONSIDERATIONS OF DEVOLATILIZATION

First we consider ideal solutions. An ideal solution is one where the solute and solvent molecules 1 and 2 have roughly the same size, shape, and force fields. An ideal solution obeys Raoult's law:

$$P_1 = Y_1 P_1^0 \tag{8.4-1}$$

where Y_1 is the mole fraction of the solute, P_1 is the vapor pressure of the solute in equilibrium with the solution, and P_1^0 is the vapor pressure of the pure solute at the given temperature. Very dilute polymer solutions exhibit nearly ideal behavior. More concentrated solutions, however, exhibit large deviations from Raoult's law. In one of the most notable early examples of polymer solution thermodynamics, Flory (12) and Huggins (13) independently dealt with this nonideal behavior. The result of this work is

the celebrated Flory–Huggins equation:

$$\ln\left(\frac{P_1}{P_1^0}\right) = \ln(1-\phi_2) + \phi_2 + \chi_{12}\phi_2^2 \tag{8.4-2}$$

where ϕ_1 and ϕ_2 are the volume fractions of the solute and the polymer, respectively, and χ_{12} is the Flory–Huggins interaction parameter for a specific polymer–solvent system. This parameter is indicative of the similarity (affinity) of the two components and can be related to the solubility parameters δ_1 and δ_2 of the solute and polymer, respectively, by the following equation

$$\chi_{12} = \frac{V_1(\delta_1 - \delta_2)^2}{RT} \tag{8.4-3}$$

where V_1 is the *molar* volume of the solvent. Solubility parameters of common polymer–solvent systems are available in the literature (2,14). Values $\chi_{12} < 0.5$ denote mutual solubility, whereas, higher values denote increasing incompatibility. With Eq. 8.4-2, the interaction parameter can be computed from experimental measurement of vapor pressure over the solution. We note that, given the interaction parameter, the limiting solute concentration for phase separation can be obtained by setting $P_1/P_1^0 = 1$. This can be observed in Fig. 8.7, which plots P_1/P_1^0 vs. ϕ_1 with χ_{12} as a parameter. We note that phase separation takes place only at $\chi_{12} > 0.5$.

At very low solute concentrations ($\phi_2 \to 1$), Eq. 8.4-2 reduces to

$$\ln\left(\frac{P_1}{P_1^0}\right) = \ln(1-\phi_2) + 1 + \chi_{12} \tag{8.4-4}$$

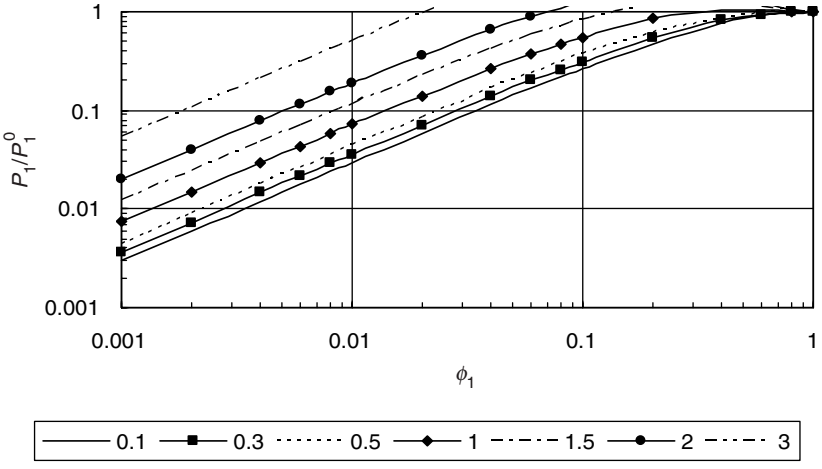

Fig. 8.7 The Flory–Huggins equation with χ_{12} as a parameter.

Equation 8.4-4 can be written with good approximation as

$$P_1 = \frac{\rho_2}{\rho_1} W_1 P_1^0 \, \mathrm{e}^{(1+\chi_{12})} \tag{8.4-5}$$

where ρ_1 and ρ_2 are the solute and polymer densities, respectively, and W_1 is the weight fraction of the solute in the solution.

Solubility is very frequently expressed in the form of Henry's law, where P_1 is proportional to the weight fraction of the solute

$$P_1 = HW_1 \tag{8.4-6}$$

and H at low concentrations becomes

$$H = \frac{\rho_2}{\rho_1} P_1^0 e^{1+\chi_{12}} \tag{8.4-7}$$

The advantage of expressing H in terms of the Flory–Huggins parameter χ_{12} is that the latter is often insensitive to temperature, and may better reflect the dependence on concentration than H. Its disadvantage is that it does not apply near and above the critical temperature of the volatile component.

If the pressure over a solution is reduced below the partial pressure of the solvent over the solution, then the solution is said to be *superheated.* The *degree* of superheat is represented by the difference between the equilibrium partial pressure of the solvent over the solution and the total pressure (vacuum level) over the solution $P_1 - P_0$. The higher the vacuum level, the higher the superheat at a given concentration and temperature. Increasing the temperature at a fixed pressure level, of course, also increases the superheat.

Simon (15) suggests that, depending on the degree of superheat, there are three rate-limiting mechanisms for devolatilization. The first he calls ''free boiling.'' This occurs at high degrees of superheat and low viscosities, namely, volatile rich conditions. Vapor bubbles are initiated at a high rate, grow, and burst. The second mechanism, he calls ''bubble growth.'' Here the superheat is lower and the viscosity is higher; consequently, the rate-determining step is bubble nucleation and growth. The third mechanism takes place at very low superheat levels where few bubbles are formed and the rate-determining step is diffusion.

Increasing the temperature of the solution and reducing the pressure above the solution as much as possible can maximize the superheat. The former is bound by the thermal sensitivity of the polymers and the latter by technical and economic factors of the vacuum generating solvent separation and condensation systems.

Example 8.1 The Degree of Superheat and Vapor Volume for a Desired Separation Level We consider a 10,000 ppm styrene–PS solution at 220°C, which has to be devolatilized to 1000 ppm. Disregarding the rate of devolatilization, we wish to determine the minimum superheat necessary in order to achieve the required separation. We assume that

$\rho_1 = \rho_2, \chi_{12} = 0.3$, and $P_1^0 = 450\,\text{kPa}$. Using Eq. 8.4-5, we first obtain the partial pressure over the solution at 10,000 ppm:

$$P_1 = (0.01) \times (450 \times 10^3) \times e^{(1+0.3)} = 16.51\,\text{kPa}$$

or 123.8 mmHg. The partial pressure over the desired solution of 1000 ppm is given by:

$$P_1 = (0.001) \times (450 \times 10^3) \times e^{(1+0.3)} = 1.65\,\text{kPa}$$

or 12.4 mmHg. Therefore the minimum degree of superheat that is required is $16.51 - 1.65 = 14.86$ kPa or 111.5 mmHg.

Next we want to calculate the volume of vapors, at 1.65 kPa and 220°C, to be removed for each kilogram of solution. We will assume that the vapor behaves as an ideal gas. For each kilogram of solution we remove 9 g of solute. The molecular weight of styrene is 104.16, and therefore we remove $9/104.16 = 0.0864$ mol, which has a volume of:

$$V = \frac{nRT}{P} = \frac{0.0864(\text{mole}) \times 8.31(\text{J/mole K}) \times (273 + 220)(\text{K})}{1650(\text{Pa})} = 0.215\,\text{m}^3$$

Example 8.2 Vacuum Staging If the volatile concentration is relatively high, removal of all the volatiles at the vacuum level needed to accomplish the desired separation will result in large vapor volumes, and hence a larger and more expensive vacuum-pumping system. In such cases, vacuum staging will be advantageous. By staging, we can remove the bulk of the volatiles at a higher pressure level (low vacuum levels) and remove the leftover volatiles at the low final pressure (high vacuum). Progressive staging becomes even more important if more than 90% removal is required.

Generally, it can be shown (1,16) that the optimum pressure profile P_j over j stage separation, which minimizes the volume of vapor when the temperature is uniform, is given by

$$P_j = P_0 a^j \qquad 1 \le j \le N$$

where

$$a = \left(\frac{P_N}{P_0}\right)^{1/N}$$

where P_j is the pressure level in stage j, and P_N is the pressure in the last stage that sets the final separation. For example, in a two-stage separation $a = (P_2/P_0)^{1/2}$, and the pressure in stage one will be $P_1 = P_0(P_2/P_0)^{1/2}$. Thus in the previous example, if in order to get the final separation we need a pressure of 1.65 kPa, than the pressure in the first stage should be $16.51(1.65/16.51)^{1/2} = 5.22$ kPa. The equilibrium weight fraction in stage one, via Eq. 8.4-5 is $W_1 = 5220/(450 \times 10^3 \times e^{(1+0.3)}) = 0.0032$. Thus, in the first stage we drop the volatile from 10,000 ppm to 3200 ppm, and in the second stage to the required 1000 ppm. From

these we can calculate the volumes to be removed in each stage, as shown in the following table:

	Feed	Stage 1	Stage 2
Weight fraction (ppm)	10,000	3200	1000
Partial pressure (kPa)	16.51	5.22	1.65
Removed weight (g/kg)		6.8	2.2
Removed (g · mol)		0.06825	0.02112
Removed volume (m^3/kg)		0.0501	0.0513

Thus, the total vapor volume to be removed in a two-stage operation is 0.1023 m^3/kg, as compared to 0.215 m^3/kg, or about one-half the volume.

8.5 DIFFUSIVITY OF LOW MOLECULAR WEIGHT COMPONENTS IN MOLTEN POLYMERS

Larry Duda and Jim Vrentas were the first to systematically study the diffusion of small molecules in molten polymers, formulate a free volume-based theoretical model, and elucidate the sharp dependence of the diffusion coefficient on temperature and concentration.[2] Figure 8.8 shows diffusivities of toluene in polystyrene as a function of concentration and temperature. The values were computed using the Vrentas and Duda (17) free volume model and, as shown, coincide well with available data.

This model, based on the earlier work of Fujita (18), currently appears to be the most effective theory to describe diffusion both above and below T_g. It adopts the notion that all transport processes are governed by the availability of free volume in the system. *Free volume* is a useful concept representing a specific volume $\hat{V}_{fv}$ present as holes of the order of molecular (monomeric) dimensions or smaller, which together with the specific volume of the molecules themselves, $\hat{V}_0$, gives the total specific volume, $\hat{V}$

$$\hat{V} = \hat{V}_0 + \hat{V}_{fv} \tag{8.5-1}$$

As the temperature above T_g decreases, the kinetic energy of chain segments decreases as well and the volume contracts, sharply reducing the relative amount of free

2. This early work was started by Larry Duda and Jim Vrentas in the 1960s at the Dow Chemical Company, in a study of styrene polymerization reactors and downstream devolatilizers, and was triggered by the lack of any reliable data on diffusion coefficients of small molecules in molten polymers. Their study continued from the 1970s on at Pennsylvania State University, where the theoretical model based on Fujita's earlier work (18) was the subject of detailed experimentation, indicating the sharp temperature and concentration dependence of the coefficient. Fujita himself became interested in the diffusion problem while working on fish drying for the Japanese fishery department, at which time he observed a strong concentration dependence of the diffusion coefficient. (Larry Duda, private communication, 2002.)

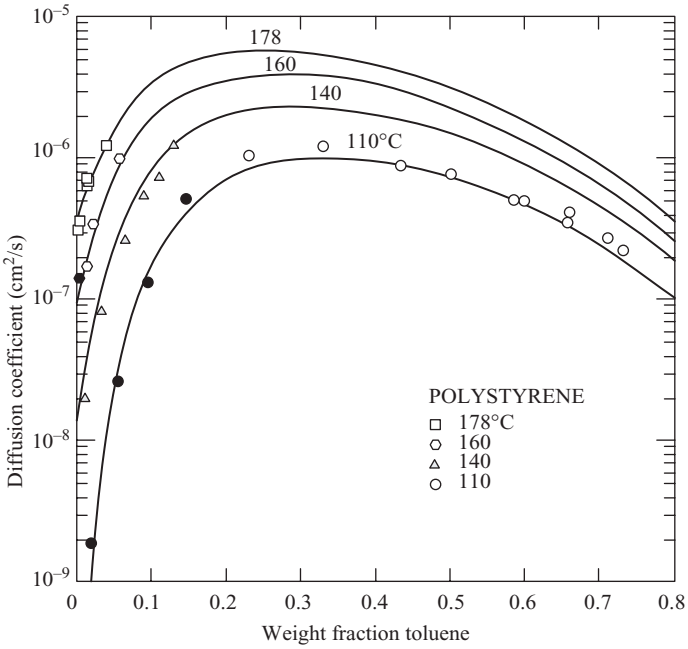

Fig. 8.8 Free volume theory prediction of mutual binary diffusion coefficient for the toluene–PS system based on parameters (19). [Reproduced by permission from J. L. Duda, J. S. Vrentas, S. T. Ju and H. T. Liu, "Prediction of Diffusion Coefficients," *A.I.Ch.E J.*, **28**, 279 (1982).]

volume between the polymeric chains approaching a constant value at T_g. Molecules diffuse by successive discrete jumps, provided a vacancy of sufficient size appears adjacent to the molecule and the molecule possesses sufficient energy to break the nearest-neighbor contacts. Assuming that the vacancy and energy availabilities are governed by a Boltzmann probability function, and that only that portion of the free volume is available for diffusion that is continuously redistributed by thermal energy, Vrentas and Duda derived the following expression for the diffusion coefficient of a solvent in polymers:

$$\mathscr{D} = (1-\phi_1)^2(1-2\phi_1\chi)\mathscr{D}_0 \exp(-E/RT) \exp\left\langle \frac{-\gamma(w_1\hat{V}_1^* + w_2\xi\hat{V}_2^*)}{\hat{V}_{fh}} \right\rangle \qquad (8.5\text{-}2)$$

where ϕ_1 is the solvent volume fraction; $\mathscr{D}_0$ is a constant preexponential term; E is the molar energy a molecule needs to overcome the attractive forces between nearest neighbors; γ is an overlap factor (between 0.5 and 1.0) to account for the fact that the same volume is available to more than one molecule; $\hat{V}_1^*$ and $\hat{V}_2^*$ are the smallest holes that need to form before a solvent and polymer segment, respectively, can make a jump; w_1 and w_2 are the weight fractions of solvent and polymer; ξ is the ratio of molar volumes for the solvent and polymer segment involved in a jump; and $\hat{V}_{fh}^*$ is the hole free volume, namely, that portion of the free volume that is available for diffusion. A detailed procedure for computing the diffusivity and evaluating the various parameters is given by Zielinski and Duda (20).

8.6 BOILING PHENOMENA: NUCLEATION

When does a liquid boil? Clearly, boiling at constant pressure—say, atmospheric pressure—begins when we increase the temperature of a liquid or solution and the vapor pressure reaches a pressure of one atmosphere. Alternatively, the pressure over a liquid or solution at constant temperature must be reduced until it reaches the vapor pressure at that temperature (e.g., vacuum distillation). Yet it is well known that liquids can be superheated (and vapors supersaturated) without the occurrence of phase transfer. In fact, liquids must *always* be superheated to some degree for nucleation to begin and for boiling to start. That is, the temperature must be raised *above* the value at which the equilibrium vapor pressure equals the surrounding pressure over the liquid, or the pressure must be reduced below the vapor pressure value. As defined earlier, these differences are called the *degree of superheat*. When the liquid is superheated, it is metastable and will reach equilibrium only when it breaks up into two phases.

There is a thermodynamic upper limit to the degree of superheat of a homogeneous liquid system, above which the metastable state cannot exist. In fact, phase separation occurs and *homogeneous boiling* begins below this limit when the *kinetic* limit of superheat is reached. This happens when bubbles begin to nucleate within the homogeneous liquid at a significant rate. Homogeneous nucleation theories, developed by Blander and Katz (21), describe a process that leads to the formation of density fluctuations in the metastable liquid, creating vapor embryos that may either grow or disappear due to vaporization or condensation, respectively. According to these theories, which are based on a vast amount of earlier work reviewed in many available texts, the rate of homogenous nucleation J takes the form:

$$J = A\, e^{(-B)} \tag{8.6-1}$$

where A and B are groupings of thermodynamic properties as given (21) in the following expression:

$$J = 3.73 \times 10^{35} \left(\frac{\rho_l^2 \sigma}{M^3 B} \right)^{1/2} \left[\exp \frac{-1.182 \times 10^5 \sigma^3}{T_0 (P_e - P_0)^2} \right] \tag{8.6-2}$$

where J (#/cm^3·s) is the rate at which nuclei are created in a unit volume; ρ_l (g/cm^3) is the density of the liquid; σ (erg/cm^2) is the surface tension; M (g/mol) is the molecular weight of the volatile component; B is a factor equal to 2/3 (and 1 for cavitation); T_0 (K) is the temperature; P_e (at) is the equilibrium vapor pressure at T_0 (K); and P_0 (at) is the pressure in the liquid. The pressure P_e is the actual pressure within the bubble and is not equal to the equilibrium vapor pressure of the liquid P_1^0. They are related as follows

$$P_e = \eta P_1^0 \tag{8.6-3}$$

where

$$\eta = \exp \frac{v_l(P_0 - P_1^0)}{RT_0} \tag{8.6-4}$$

where v_l is the specific volume of the liquid.

The resulting expression, Eq. 8.6-2, has a weak temperature-dependent preexponential term, and a temperature sensitive exponential term. The latter contains the surface tension to the third power and the superheat to the second power. With increasing temperature the surface tension drops, and superheat increases, giving rise to an increase of orders of magnitude in J over a very narrow temperature range.

The computed kinetic limit of superheat of *n*-butane, for example, is 378.3 K and the experimentally measured[3] value is 376.9 K. With ordinary liquids, the kinetic limit of superheat approaches the critical temperature ($T_{\text{kls}}/T_{\text{crit}} = 0.89$). However, under ordinary conditions, when the liquid is in contact with solid surfaces, it boils far below the kinetic limit of superheat. Thus, the boiling point of *n*-butane, for example, is 272.5 K. Similarly, the theoretical kinetic superheat of water is 300°C, while the ordinary boiling point of water is 100°C.

When the vapor phase is generated at a solid interface rather than in the bulk of the liquid, the process is known as *heterogeneous nucleation.* Heterogeneous nucleation theories on smooth surfaces yield similar expression to Eq. 8.6-1 for J, with modified groupings A' and B' that account for the contribution of geometry and energy of the solid surface (22).

Smooth surfaces in and of themselves do not substantially reduce the kinetic limit of superheat. However, ordinary surfaces have macroscopic and microscopic scratches—gouges, grooves, and pits of the order of 1–5 μm—and the preexistence of gas or vapor phases in these surface imperfections generates the nuclei in heterogeneous boiling. If the surfaces are not perfectly wetted by the liquid, as the case usually is, it may be expected that many of these cavities will contain entrapped gas, and hence act as bubble initiators, thereby reducing the kinetic limit of superheat to negligibly small values. Hence, the common experience that boiling starts at the solid wall of any kettle (where the superheat is even higher due to the outside heating sources).

Indeed, it has been proven experimentally that, if prior to heating, the liquid is pressurized to very high pressures, thereby dissolving the gas in these cavities into the liquid, the superheat needed for nucleation increases dramatically. Of course, in the presence of these bubble-generating cavities, the degree of superheat needed for boiling is significantly reduced. In addition, a liquid saturated at a given temperature (say at room temperature) with a gas such as air, will activate additional bubbles with increasing temperature, as a result of decrease in solubility with increasing temperature. The same happens when the pressure is reduced over a supersaturated and pressurized liquid, as is the case when a soda bottle is opened.

Finally, it is worth mentioning that the *cavitation* phenomenon observed in low viscosity liquids is also caused by (explosive) boiling induced by sudden reduction of pressure, such as that occurring in regions behind moving surfaces, such as impellers, or as the result of flow acceleration (Bernoulli effect) (23).

3. A common method to measure the kinetic limit of superheat is by the exploding drop technique. In this technique a small droplet of the liquid is placed in a column of another immiscible liquid and either the temperature is raised until homogenous boiling begins or the pressure is reduced.

8.7 BOILING–FOAMING MECHANISMS OF POLYMERIC MELTS

The devolatilization process of polymeric melts is generally a boiling–foaming[4] mechanism that takes place within the bulk of the homogenous liquid phase. Thus, one would expect that homogenous nucleation theories should be applicable to devolatilization. However, these theories fail to give a satisfactory explanation for the boiling–foaming process at the temperature and pressures at which it is practiced. These theories for polystyrene–styrene systems, for example, predict that degrees of superheat far in excess of processing temperatures are required to attain observed nucleation rates. In fact, heterogeneous nucleation theories are not useful in predicting the experimental observation, either. Moreover, bubbles resulting from heterogeneous nucleation at the solid containing walls would by and large remain close to the wall and will not move quickly into the bulk because of the very high viscosities of the melt. The same holds true for bubbles originating from entrapped gasses and vapors in wall cavities and scratches, which are the major sources of heterogonous nucleation under ordinary conditions.

What, then, is the nucleation mechanism in the bulk of these viscous molten polymer solutions?

In a polymeric system, it would be reasonable to examine the possibility that the free volume concept described earlier, which explains so well phenomena like molecular diffusion and viscosity, might perhaps also explain nucleation phenomena. The critical radius r_e of a stable bubble can be obtained from a simple mechanical-force balance, yielding the Laplace equation:

$$r_e = \frac{2\Gamma}{P_e - P_0} \tag{8.7-1}$$

where Γ is the surface tension. Bubbles smaller than r_e will shrink and disappear and larger ones will grow. For a devolatilizing system of, say, 1000–10,000 ppm styrene in polystyrene (PS), the critical radius can be shown to be of the order of 1–12 μm (24). However, the free volume theories involve holes of the order of molecular dimensions and, as shown by Lee and Biesenberger (24) and Lee (25), the probability of finding free volume of the critical bubble size approaches zero.

Any explanation of nucleation in polymer melts at devolatilization conditions must also explain the experimental observation of the catalytic effect of shearing on bubble nucleation, whereby profuse foaming starts with the slightest shearing. Lee and Biesenberger investigated this phenomenon in some detail. They concluded that a melt saturated with entrained bubbles in a rolling-pool configuration, shown in Fig. 8.6(b), foams immediately following the application of vacuum, without being agitated or experiencing deformation. Otherwise, deformation, however slight, is required in addition to positive superheat (24). In deformation-induced nucleation, one should consider the possibility that shearing flow, which normally exists in devolatilizers, might shift the distribution of free volume toward the large end to give reasonable

4. The term foaming comes from the fact that the melt is very viscous and, when the devolatilization process begins, the melt fills up with bubbles that appear as foam. Sometimes, as in foaming processes, low boiling-point additives are added to enhance the process.

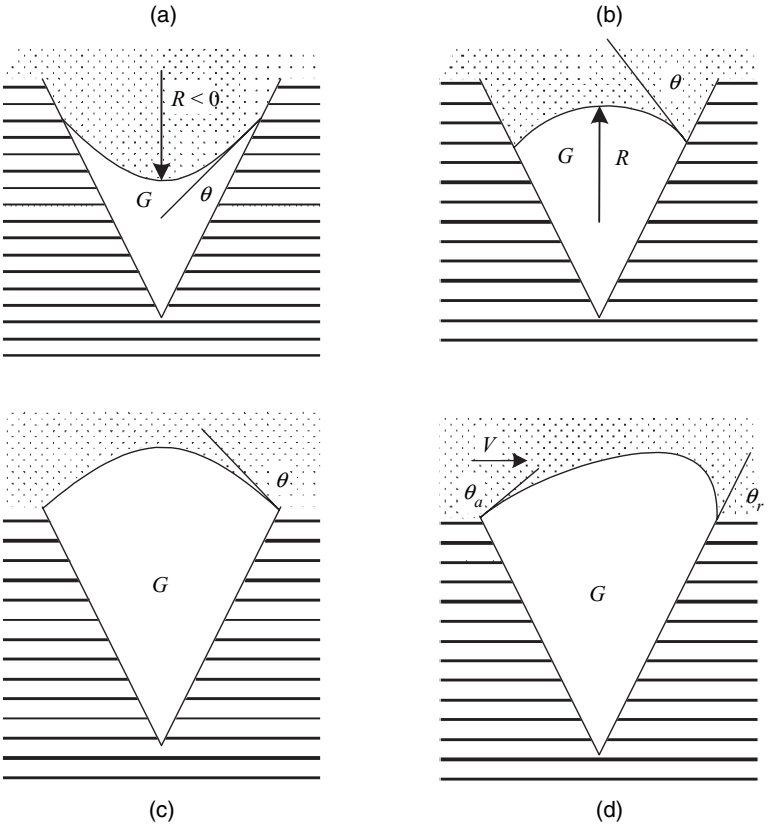

Fig. 8.9 Schematic representations of metastable cavity models.

probability for the existence of holes of the critical dimensions. However, Lee and Biesenberger ruled out this possibility as well, on the ground that very low shearing rates, well within the Newtonian range, sufficed to produce swarms of bubbles in their experiments.

They suggested explaining bubble nucleation by the preexistence of Harvey-type[5] (26) heterogeneous germ-nuclei, or free-streaming nuclei, located within the cracks and crevices of microscopic particulate matter believed to be present in all liquids. It presumes that within these acute-angle cracks and crevices, pockets of gas or vapor can exist in equilibrium within the liquid indefinitely, until activated by superheat and shearing. Figure 8.9 illustrates conical-shaped crevices and various alternative configurations of gas pockets with negative and positive radii of curvature. In the former case, the surface tension partly supports the pressure of the liquid, and the pressure within the pocket, according to Eq. 8.7-1, is less than that in the liquid: $P_e < P_0$. The deeper the penetration, the smaller the radius of curvature will be, and the lower the pressure in the gas pocket will be, until an equilibrium state with the liquid prevails and stable pockets are created.

5. During World War II Harvey et al. investigated the well-known phenomenon of bubbles appearing in the blood and tissue of divers surfacing too quickly after deep diving.

Alternatively, it can be argued, as did Harvey et al., that the contact angle between the liquid and the hydrophobic surface in this case can reestablish itself as the meniscus moves, due to absorption or release of vapor, and therefore it is unstable. This could explain the existence of relatively large, stable pockets of vapor and/or air dispersed within the melt. Lee and Biesenberger (24) estimated that pockets of the size of 1μm could exist in the melt, and these fall within the range of critical nuclei for bubble formation. When superheat is applied, the pressure within the pockets exceeds that in the liquid and the radius of curvature becomes positive, as in Fig. 8.9(b) and 8.9(c).

Harvey et al. further argued that in order to detach a gas pocket from the solid surface, it is necessary to reduce the receding angle θ_r below a critical value. This, claim Lee and Biesenberger, implies a yield phenomenon that occurs when the pocket is swollen to the cavity mouth, where contact angles are likely to experience a sharp increase and dislodge the gas/vapor phase into a bubble [Fig. 8.9(d)]. Possibly, the role of shear in inducing nucleation may be related to this phenomenon. Indirect support for this proposition comes from their experimental work with LDPE and CCl_2F_2 as a volatile foaming agent, which revealed that the number of bubbles formed per unit volume increased linearly with the capillary number, expressing the ratio of laminar flow-induced shear forces on the bubble-to-surface tension forces (27):

$$\mathrm{Ca} = \frac{R\mu\dot{\gamma}}{\Gamma} \tag{8.7-2}$$

where μ is the melt viscosity, Γ the surface tension, and $\dot{\gamma}$ the shear rate.

As in devolatilization, Harvey-type free-streaming nuclei are also invoked in explaining cavitation nucleation in water and low viscosity liquids. Brennen (28) points out that ''many of the observations of the onset of cavitation appear to be the result of free stream nuclei rather than surface nuclei.'' Indeed, he points out that cavitation nuclei number density distributions were measured by holography in water tunnels. This method, however, does not distinguish between the solid particles and microbubbles that may be present in the liquid, and the exact character of these free-streaming nuclei still needs to be elucidated. Moreover, a rather esoteric suggestion was made regarding continuous production of nuclei by cosmic radiation. Yet, Greenspan and Tschiegg (29) showed that removal of particles larger than 0.2 μm from water raised its tensile strength to 200 bar, and Marschall et al. (30) showed that incorporating small spherical hydrophobic particles into the water significantly reduced the tensile strength of purified water. Furthermore, it was shown that imposing high pressure on water, which presumably dissolves the entrained gas pockets and destroys the nuclei, raises the tensile strength and kinetic limit of superheat of water. All this evidence seems to support the free-streaming nuclei theory, though no direct experimental observations on their nature have yet been made.

In devolatilization with viscous polymeric melts, it is difficult, of course, to carry out similar experiments and prove indirectly that free-streaming nuclei may play a similar role, but microscopic particles originating from the monomers and catalyst systems are likely to be found in the polymeric product. Moreover, it is well known that the addition of fine powders and solid particles induces foaming. Therefore, the Biesenberger–Lee proposition seems plausible.

As mentioned earlier, entrained free air cannot survive indefinitely in a liquid, but it can still play a role in the devolatilization process in rotary machinery, where the moving surface can drag free air into the melt, forming small bubbles that can serve as nuclei for

further bubble growth. At atmospheric pressures, air entrainment takes place at a critical modified capillary number of 1.18 (31):

$$\mathrm{Ca} = \frac{\mu V}{\Gamma} \tag{8.7-3}$$

where V is the velocity of the solid surface. According to this criterion high viscosity induces gas entrainment, but it is questionable if this criterion holds at low pressures.

8.8 ULTRASOUND-ENHANCED DEVOLATILIZATION

In devolatilization, the superheat for nucleation and boiling, at a fixed temperature, is set by the absolute pressure (vacuum) that can be attained. The upper limit of the superheat is attained by setting absolute pressure to zero. Triaxial stretching of a liquid may reduce the ambient pressure to negative values. That can be achieved by imposing the liquid to an ultrasonic source. The acoustic field causes high-frequency stretching–compression stresses within the liquid which, in ordinary liquids, can result in bubble nucleation and acoustic cavitations (23). The bubble nucleation rate may be catalyzed by ultrasonic fields, possibly both as a result of the increased instantaneous superheat and the imposed deformation, which might overcome the yielding of the Harvey-type activated nuclei, as was suggested in shear fields. Tukachinsky et al. (32) studied the effect of ultrasonic fields on polymer strand devolatilization and observed a significant increase in separation, as shown in Fig. 8.10.

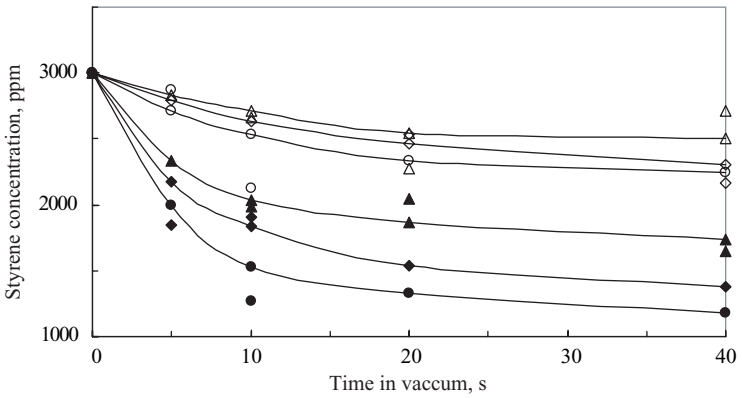

Fig. 8.10 Residual styrene concentration in PS extruded at 225°C. The open symbols refer to experiments without ultrasound, while the filled ones refer to experiments where ultrasound radiation was applied. The parameter is the absolute pressure in the chamber. Triangles: 150 mmHg; squares: 50 mmHg, and circles: 12 mmHg. [Reprinted by permission from A. Tukachinsky, Z. Tadmor, and Y. Talmon, ''Ultrasound-enhanced Devolatilization in Polymer Melt,'' *AIChE J*., **39**, 359 (1993).]

8.9 BUBBLE GROWTH

Once a nucleus of a critical size is formed in a superheated solution, the volatile component in the liquid phase begins diffusing to the interface and vaporizing into the vapor space. Consequently the pressure in the bubble increases, and it will begin to grow in size. The rate of bubble growth is a complex and unsteady process affected by diffusion, heat transfer, and viscous forces. Depending on the system and conditions, one or more of these transport operations may be the rate-controlling step. Favelukis and Albalak (33) review a spectrum of solutions proposed in the literature for a single spherical bubble in a quiescent superheated Newtonian liquid of infinite extent, and discuss their relevance or rather lack of relevance to devolatilization. The latter is due to the fact that in devolatilization of polymeric liquids the liquid is non-Newtonian, there are swarms of bubbles, the liquid is sheared and therefore the bubbles are deformed, and, more importantly, microscopic studies, discussed below, indicate a far more complex mechanism than simple diffusion into the surface of a growing bubble.

Nevertheless, in order to get some insight into the mechanism of bubble growth, and following the classic derivation of Scriven (34), we derive here the particular case for the rate of growth of a single bubble in a quiescent infinite liquid (Fig. 8.11), with the viscous forces acting as the rate-controlling step.

The equation of continuity for an incompressible liquid, and with spherical symmetry, reduces to

$$\frac{\partial}{\partial r}\left(r^2 v_r\right) = 0 \tag{8.9-1}$$

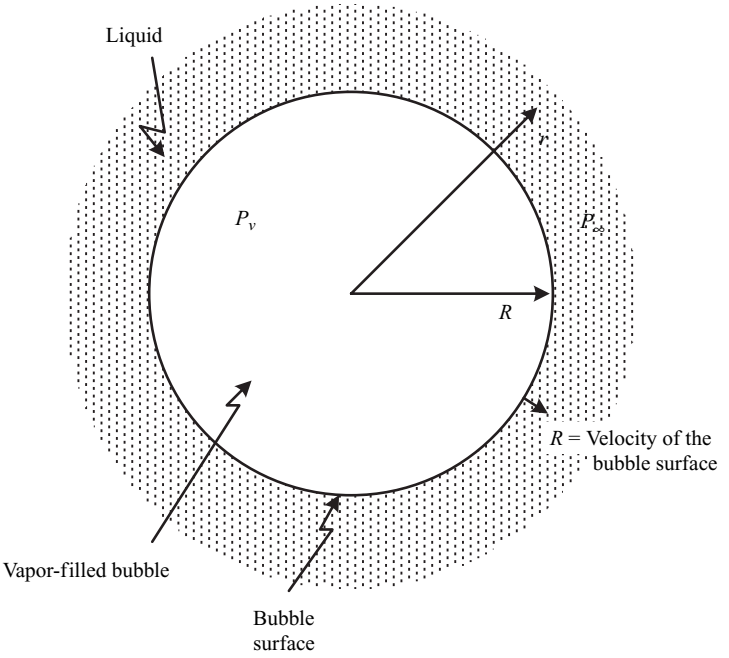

Fig. 8.11 Diffusion of volatiles into a growing bubble of radius R. The pressure inside the bubble is P_v, the pressure in the liquid far from the bubble surface is P_∞, the bubble surface is moving radially at velocity $\dot{R}$.

which can be integrated to give

$$v_r r^2 = f(t) \tag{8.9-2}$$

Since $v_r r^2$ is a function of time alone, it must hold everywhere in the liquid, including at the surface of the bubble. The surface itself moves at velocity $\dot{R}$, while the liquid adjacent to the surface moves with velocity $v_r(R)$, which is different from that of the surface because some of the volatile material evaporates, and the mass flow rate is given by $4\pi R^2 \rho_L \left[\dot{R} - v_r(R)\right]$, which is the rate of vaporization of volatile material into the bubble. We now can write a mass balance over the bubble surface:

$$\frac{d}{dt}\left(\frac{4}{3}\pi R^3 \rho_G\right) = 4\pi R^2 \rho_L \left[\dot{R} - v_r(R)\right] \tag{8.9-3}$$

where ρ_L and ρ_G are the densities of the gas and liquid phases, respectively. Assuming constant density of the gas in the bubble Eq. 8.9-3 reduces to

$$v_r(R) = \dot{R}(\rho_L - \rho_G)/\rho_L = \varepsilon \dot{R} \tag{8.9-4}$$

Equation 8.9-2 suggests that the product of the radial velocity and the square of the radius is constant anywhere in the liquid phase, which gives the following continuity condition:

$$v_r r^2 = \varepsilon \dot{R} R^2 \tag{8.9-5}$$

Next we turn to the Navier–Stokes equation, which for creeping flow of incompressible liquids, neglecting inertial and gravitational forces, reduces to

$$0 = -\frac{\partial P}{\partial r} + \mu\left[\frac{1}{r^2}\frac{\partial^2}{\partial r^2}\left(r^2 v_r\right)\right] \tag{8.9-6}$$

Substituting Eq. 8.9-5 into Eq. 8.9-6 and integrating over the radius from the bubble surface to infinity results in

$$\frac{\partial P}{\partial r} = 0 \tag{8.9-7}$$

which after integrating from the surface of the bubble to infinity, gives

$$P_\infty - P_R = 0 \tag{8.9-8}$$

where P_∞ is the ambient pressure, and P_R is the pressure in the *liquid* phase at the bubble surface. Next we make a force balance at the bubble surface, much like with the Laplace

equation, but for this case involving bubble growth, we must add the viscous forces to the pressure drop to give

$$P_B - P_R - \tau_{rr} = 2\Gamma/R \tag{8.9-9}$$

where P_B is the uniform pressure in the bubble, Γ is the surface tension, and τ_{rr} is the radial component of the viscous stress tensor in the liquid, given by

$$\tau_{rr} = -2\mu \frac{\partial v_r}{\partial t} \tag{8.9-10}$$

Substituting Eq. 8.9-8 and Eq. 8.9-10 into Eq. 8.9-9 results in:

$$P_B - P_\infty - \frac{2\Gamma}{R} = \frac{4\mu}{R}\left(\frac{dR}{dt}\right) \tag{8.9-11}$$

which is a special case of the Rayleigh equation with the inertial terms neglected. At constant ambient and bubble pressure, Eq. 8.9-11 may be integrated with the initial condition of $R = R_0$ at time zero:

$$R(t) = R_{cr} + (R_0 - R_{cr})\left[\exp\frac{(P_B - P_\infty)t}{4\mu}\right] \tag{8.9-12}$$

where

$$R_{cr} = \frac{2\Gamma}{P_B - P_\infty} \tag{8.9-13}$$

is the equilibrium critical radius of the bubble in the absence of viscous forces.

We therefore find that in this special case the bubble radius grows exponentially in time. The pressure drop is a forward-driving force for bubble growth and viscosity is a retarding force.

8.10 BUBBLE DYNAMICS AND MASS TRANSFER IN SHEAR FLOW

Much of the devolatilization takes place in rotating machines where, by and large, the bubbles formed are exposed to a shear field. We must therefore consider the effect of shear fields on bubble shape and mass transfer. It has been shown that the deformation of a bubble (inviscid droplet) in a Newtonian liquid in simple shear creeping flow is governed by a single dimensionless parameter, the capillary number Ca, expressing the ratio of shear to surface tension forces, defined in Eq. 8.7-2 with the equivalent radius a (radius of a sphere of equal volume) replacing R. At small deformations ($\mathrm{Ca} \ll 1$) the bubble becomes an ellipsoid, oriented along

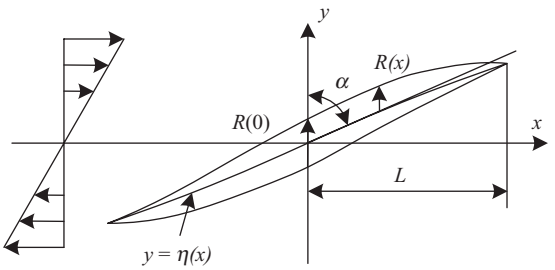

Fig. 8.12 Deformation of a bubble in simple shear flow at Ca $\gg$ 1. $R(x)$ is the bubble radius as a function of coordinate x; L is the half-length of the bubble; α is the inclination angle; and $y = \eta(x)$ is the position of the bubble centerline.

the principal axis of deformation of the undisturbed flow, with the G.I. Taylor deformation parameter D, equaling the capillary number Ca

$$D = \frac{l - b}{l + b} = \mathrm{Ca} \tag{8.10-1}$$

where l and b are, respectively, the major and minor axes of the ellipse inclined 45° in the direction of flow.

In devolatilizing systems, however, Ca $\gg$ 1 and the bubbles deform into slender S-shaped bodies, as shown in Fig. 8.12. Hinch and Acrivos (35) solved the problem of large droplet deformation in Newtonian fluids. They assumed that the cross section of the drop is circular, of radius a, and showed that the dimensionless bubble surface area, A^*, defined as the ratio of the surface area of the deformed bubble A to the surface area of a spherical bubble of the same volume, is approximated by (36):

$$A^* = \frac{A}{4\pi a^2} = 1.41\,\mathrm{Ca}^{1/4} \tag{8.10-2}$$

and the dimensionless half-length of the bubble L^*, and the slenderness ratio $R^*(0)/L$, where $R^*(0)$ is the dimensionless radius of the cross section at the center,

$$R^*(0) = \frac{R(0)}{a} = 0.578\,\mathrm{Ca}^{-1/4} \tag{8.10-3}$$

are given, respectively, by

$$L^* = \frac{L}{a} = 3.45\,\mathrm{Ca}^{1/2} \tag{8.10-4}$$

and

$$\frac{R^*(0)}{L^*} = \frac{R(0)}{L} = 00.167\,\mathrm{Ca}^{-3/4} \tag{8.10-5}$$

Canedo et al. (36) confirmed these predictions for bubbles in a Couette flow apparatus.

Favelukis et al. (37,38) dealt with the problem of droplet deformation in extensional flow with both Newtonian and non-Newtonian Power Law model fluids, as wellas bubble breakup. For the Newtonian case, they find that as an inviscid droplet (or bubble) deforms, the dimensionless surface area is proportional to the capillary number

$$A^* = \frac{10}{3}\mathrm{Ca} \tag{8.10-6}$$

Thus, extensional flow is more efficient in increasing surface area as compared to shear flow.

The breakup or bursting of liquid droplets suspended in liquids undergoing shear flow has been studied and observed by many researchers beginning with the classic work of G. I. Taylor in the 1930s. For low viscosity drops, two mechanisms of breakup were identified at critical capillary number values. In the first one, the pointed droplet ends release a stream of smaller droplets termed ''tip streaming''; whereas, in the second mechanism the drop breaks into two main fragments and one or more satellite droplets. Strictly inviscid droplets such as gas bubbles were found to be stable at all conditions. It must be recalled, however, that gas bubbles are compressible and soluble, and this may play a role in the relief of hydrodynamic instabilities. The relative stability of gas bubbles in shear flow was confirmed experimentally by Canedo et al. (36). They could stretch a bubble all around the cylinder in a Couette flow apparatus without any signs of breakup. Of course, in a real devolatilizer, the flow is not a steady simple shear flow and bubble breakup is more likely to take place.

Bubble deformation in shear flow increases mass transfer because of the increase in surface area and because of convection. The latter brings volatile-rich liquid to the bubble surface. Favelukis et al. (39) studied the (identical but experimentally easier) reverse problem of *dissolution* of a gas bubble in a sheared liquid, both theoretically and experimentally, and they confirmed the increase of mass transfer with increasing shear rate. They also showed that the rate of dissolution, da/dt, where a is the equivalent radius of the bubble, is given by

$$\frac{da}{dt} \approx -\frac{RT(C_s - C_\infty)}{P}\mathscr{D}^{1/2}\dot{\gamma}^{1/2} \tag{8.10-7}$$

for a nearly spherical bubble ($\mathrm{Ca} \ll 1$), and by:

$$\frac{da}{dt} \approx -\frac{RT(C_s - C_\infty)}{P}\mathscr{D}^{1/2}\dot{\gamma}^{3/8}a^{-1/8}\left(\frac{\mu}{\Gamma}\right)^{-1/8} \tag{8.10-8}$$

for a slender bubble ($\mathrm{Ca} \gg 1$), where R is the universal gas constant, T is the absolute temperature, C_s is the concentration of the gas at the interface, and C_∞ is the concentration gas far from the interface, P is the bubble pressure, $\mathscr{D}$ is the diffusivity, $\dot{\gamma}$ is the shear rate, μ is the viscosity, and Γ is the surface tension. Clearly, the rate of dissolution increases significantly at large Ca numbers with 3/8 power of the shear rate. The same should be expected for bubble growth, and hence one could conclude that devolatilization efficiency ought to improve with increasing rotational speed.

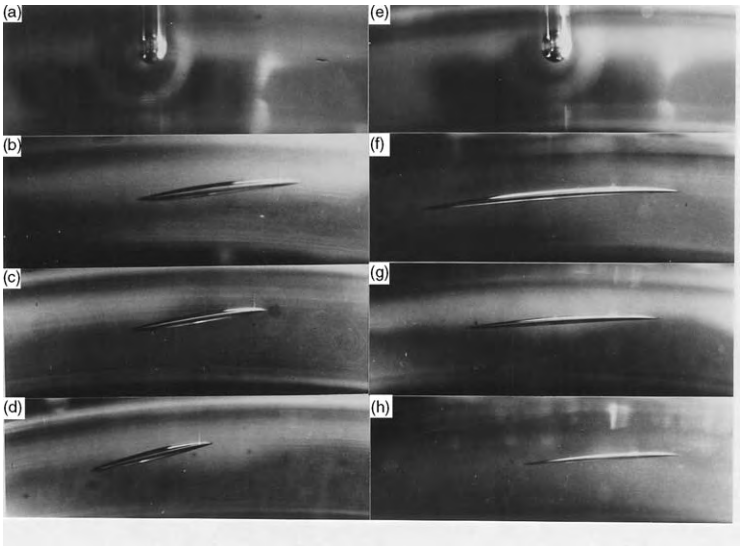

Fig. 8.13 Photograph of bubble deformation and bubble dissolution, in simple shear flow at room temperature, in a Newtonian low molecular-weight polyisobutylene (Chevron PB 24), in a Couette flow apparatus. Left: shear rate 5.5 s^{-1}, (a) $t = 0$ min, $a = 1.2$ mm; (b) $t = 1.5$ min, $a = 1.14$ mm; (c) $t = 5.5$ min, $a = 0.98$ mm; (d) $t = 7.5$ min, $a = 0.92$ mm. Right: shear rate 16.6 s^{-1}; (e) $t = 0$ min, $a = 1.2$ mm; (f) $t = 1.1$ min, $a = 1.15$ mm; (g) $t = 5.1$ min, $a = 0.93$ mm; (h) $t = 8.0$ min, $a = 0.80$ mm: [Reprinted by permission from M. Favelukis, Z. Tadmor, and Y. Talmon, "Bubble Dissolution in Viscous Liquids in Simple Shear Flow," *AIChE J.*, **41**, 2637 (1995).]

Figure 8.13 shows the dissolution of bubbles in simple shear flow as a function of time and shear rate, confirming Eq. 8.10-7.

8.11 SCANNING ELECTRON MICROSCOPY STUDIES OF POLYMER MELT DEVOLATILIZATION

Albalak et al. (40) were the first to experimentally examine the devolatilization mechanism on a microscopic scale, and their results revealed a far more complex and subtle mechanism than what was expected by the straightforward foaming–boiling process they observed. PS with a known content of styrene was extruded in a modified melt-flow indexer. The thin melt strand was extruded into a temperature-controlled brass chamber connected to a vacuum pump, and after a prescribed time, was frozen by a spray of cooling water. After freezing, scanning electron micrograph (SEM) samples were prepared to examine the surface and the fractured cross section of the strands. The PS contained 2300 ppm styrene and was extruded in the temperature range of 170–235°C. The partial pressure of a 2300 pp styrene–PS solution at 170°C is of the order of 4 kPa (30 mmHg), and at 235°C, is 12 kPa (90 mmHg). Figure 8.14 shows a control sample extruded at 180°C into atmospheric pressure with no signs of foaming (as would be expected in the absence of superheat). However, when the strands were extruded into a high vacuum that created the necessary superheat for boiling, a series of characteristic features were observed. We discuss these in the following subsections.

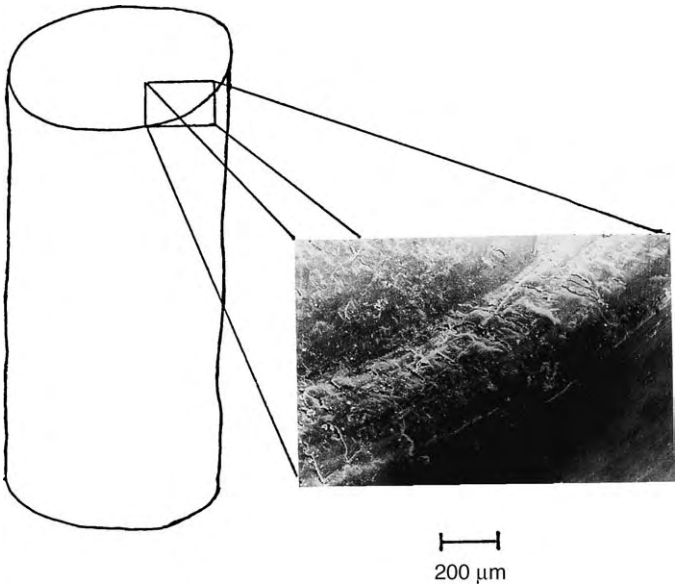

Fig. 8.14 PS–styrene sample extruded at 180°C into atmospheric pressure. The micrograph shows the smooth lateral surface and part of the cross section; there is no evidence of bubbles. [Reprinted by permission from R. J. Albalak, Z. Tadmor, and Y. Talmon, "Scanning Electron Microscopy Studies of Polymer Melt Devolatilization," *AIChE J.*, **33**, 808–818 (1987).]

Macrobubbles

The first characteristic morphological feature was the appearance of *macrobubbles*, relatively large voids, randomly scattered spatially, of the order of 100 μm and above. These are shown on the lateral surface and cross section of the sample in Fig. 8.15. Postulating that the macrobubbles have their origins in outside sources, such as entrapped noncondensable gases or moisture, the authors concluded that they are the final stage of a growth process of vapor-filled bubbles in the natural course of boiling, as discussed later in this section.

Blisters

Perhaps the most striking morphological feature discovered were swarms of *blisters* on the inner surface of the macrobubbles, located both on the lateral surface and within the core of the strand, as shown in Figs. 8.16 and 8.17, respectively. These are thin, dome-shaped, vapor-filled pockets attached to the soft inner surface of the large macrobubbles. There are two types of blisters: *microblisters*, ranging in size from 1 to 3 μm diameter, and *miniblisters*, ranging in size from 10 to 15 μm diameters. Figure 8.17 shows microblisters and miniblisters side by side. The researchers hypothesized that this arrangement is not coincidental and that the miniblisters actually evolve from the microblisters. They suggested that a first generation of microblisters emerges through the soft surface of a macrobubble after having been formed as tiny boiling nuclei that grow into microbubbles under the surface. Being close to the surface in a melt that possesses significant tensile

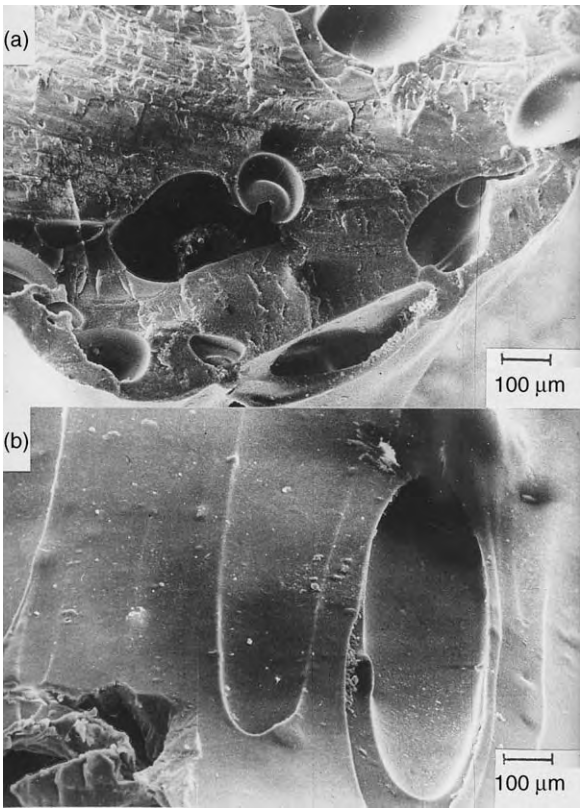

Fig. 8.15 PS–styrene sample extruded into 100-Pa pressure. (a) Cross section (170°C); (b) Lateral surface (180°C). Large macrobubbles are evident over both surfaces. [Reprinted by permission from R. J. Albalak, Z. Tadmor, and Y. Talmon, ''Scanning Electron Microscopy Studies of Polymer Melt Devolatilization,''*AIChE J*., **33**, 808–818 (1987).]

strength, these microbubbles naturally develop into blisters (much like when a stream of air is blown into a soap solution).

Once the newly formed styrene–vapor-filled microblisters grow to a maximum diameter of about 3 μm, at which stage the skin containing the vapor is too thin and weak to withstand the pressure difference, they burst, releasing the contained vapor into the macrobubble. This behavior is characteristic of microblisters that happen to break to the surface at relatively large distances (>8μm) from each other. However, microblisters emerging closer to each other may merge to form a larger ''miniblister'' with a slightly thicker skin than that of the original microblister. In this manner, adjacent microblisters combine to form miniblisters, as clearly evident in Fig. 8.17. At some later stage, miniblisters also burst and the skin collapses, entraining small vapor-filled pockets that form nuclei for a new generation of microblisters, as can be clearly seen in Fig. 8.18.

According to this hypothesized mechanism, the process has an autocatalytic feature in that the bursting micro- and miniblisters create many new nuclei for new generations of microblisters. Moreover, the subsequent, quickly expanding macrobubble creates tensile

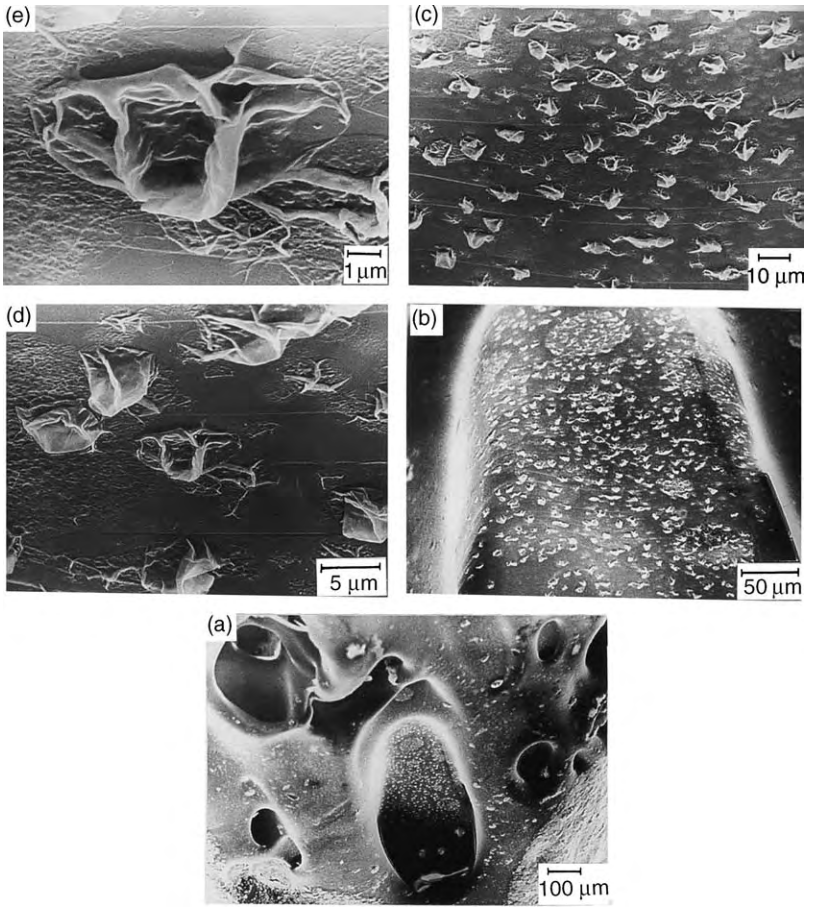

Fig. 8.16 Blisters in a macrobubble on the area of the lateral surface of a PS–styrene sample extruded at 200°C into 200-Pa pressure. (a) Lowest magnification shows macrobubbles and blister-covered inner surface. (b) Inner surface of macrobubbles at large magnification. (c) and (d) Randomly scattered collapsed blisters at increasing magnification, respectively. (e) A single collapsed blister. [Reprinted by permission from R. J. Albalak, Z. Tadmor and Y. Talmon, ''Scanning Electron Microscopy Studies of Polymer Melt Devolatilization,''*AIChE J.*, **33**, 808–818 (1987).]

stress on the inner surface of the macrobubble, further accelerating the nucleation of new microbubbles under the soft surface. Thus, perhaps it is no wonder that such a 'blistering' devolatilization mechanism would yield relatively few macrobubbles at the expense of the rest of the core material.

Microblister Remains: Hair-like Fibers, Crusty Nodules, Stringy Fibers, and Spongy Surfaces

As the volatile content of the polymer is depleted, the blisters undergo a series of fascinating transformations until they fade away into the featureless soft inner surface of

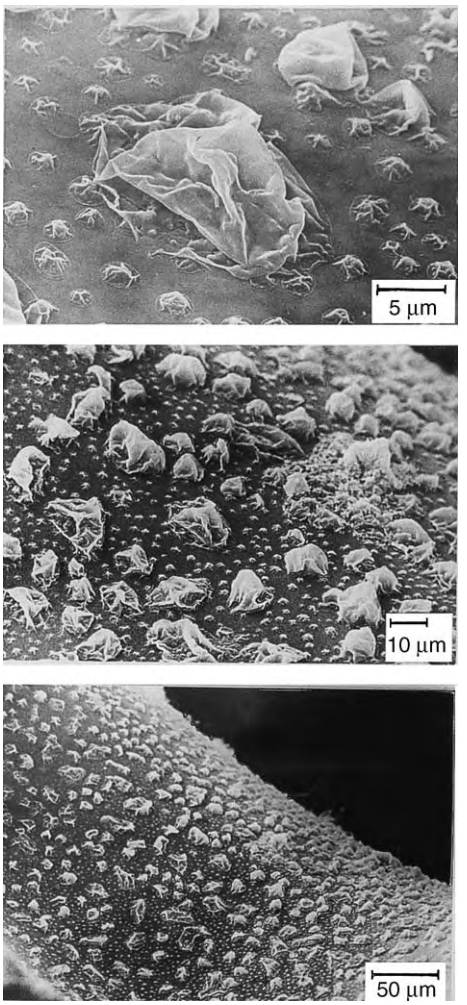

Fig. 8.17 Blisters in a macrobubble in the core of the strand of a PS–styrene sample extruded at 235°C into 300-Pa pressure. These magnifications show miniblisters and microblisters on the inner surface of a macrobubble within the core of the strand. [Reprinted by permission from R. J. Albalak, Z. Tadmor, and Y. Talmon, ''Scanning Electron Microscopy Studies of Polymer Melt Devolatilization,'' *AIChE J.*, **33**, 808–818 (1987).]

the macrobubble. Like the blisters, these are transient forms that quickly fade during the devolatilization process. Among the features observed were *hair-like fibers* that were 0.1–0.2 μm thick and about 3–5 μm long; *crusty nodule-like* structures; stringy fiber-like structures; spongy surfaces consisting of holes of about 1–3 μm.

The morphology remaining in a blister-inhabited area subsequent to the depletion of the volatile is shown in Fig. 8.19. The large circular tracks are those of miniblisters, while the smaller ones are those of the microblisters. Not all macrobubbles show the presence of blisters. Clearly, in the devolatilization process, after the volatiles are depleted

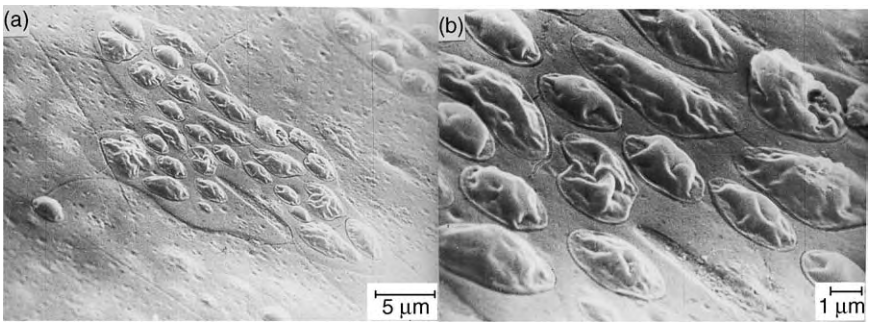

Fig. 8.18 Lateral surface of PS–styrene sample extruded at 170°C into 100-Pa pressure. Two magnifications of the same area show microblisters growing on the remains of collapsed miniblisters. [Reprinted by permission from R. J. Albalak, Z. Tadmor, and Y. Talmon, ''Scanning Electron Microscopy Studies of Polymer Melt Devolatilization,'' *AIChE J.*, **33**, 808–818 (1987).]

and before freezing of the samples took place, the surface might have healed itself to become smooth and featureless.

The preceding observations on the microscopic features of polymer melt devolatilization are not unique to the PS–styrene system, or to strand devolatilization. Similar, though somewhat less rich, features of blister-covered macrobubbles were observed with low-density polyethylene (PE), high-density PE and polypropylene (PP) systems (40,41). Furthermore, Tukachinsky et al. (11) discovered macrobubbles covered with microblisters in a 50-mm-diameter vented SSE, with PS showing more oblong shapes as a result of shearing. The onset of foaming with the application of vacuum was quicker with increased frequency of screw rotation, and the separation was more efficient.

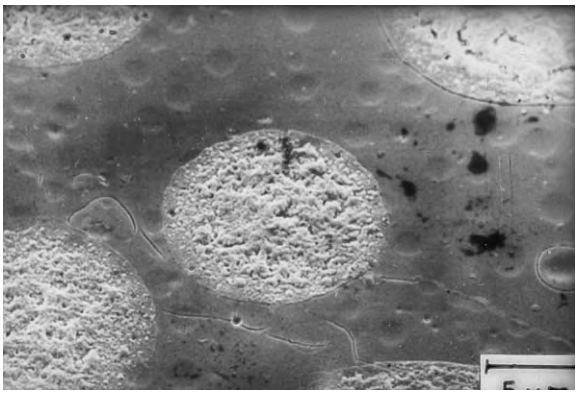

Fig. 8.19 Strand cross section of a PS–styrene sample extruded at 170°C and 100-Pa pressure. Coarse circular areas are the remains of miniblisters; small circular indentations are those of microblisters. [Reprinted by permission from R. J. Albalak, Z. Tadmor, and Y. Talmon, ''Scanning Electron Microscopy Studies of Polymer Melt Devolatilization,'' *AIChE J.*, **33**, 808–818 (1987).]

The foaming–boiling mechanism described previously may be characteristic not only to polymeric melts, but it may also be the inherent boiling mechanism of viscoelastic liquids in general.

Theoretical Formulation

Clearly, this mechanism is more complex than ordinary boiling mechanisms, and any theoretical formulation of devolatilization must take into account this complexity. An initial attempt to formulate semiquantitative elements of this mechanism was made by Albalak et al. (41). They proposed that once a nucleus of a macrobubble is created and the bubble begins to grow, the stretched inner surface of the bubble enhances the rate of nucleation just beneath the soft surface, thus generating new blisters, as shown schematically in Fig. 8.20.

Turning to Eq. 8.6-2, we note that the superheat appears in the denominator of the exponent term. As pointed out earlier, under ordinary conditions the maximum superheat of a given system at a fixed temperature can be obtained by reducing P_0 to a minimum value close to zero. However, further decrease in the local value of P_0 can be obtained by a cavitation process due to the tensile stresses generated in the moving boundaries of the macrobubble. Street (42) showed that the bubble surface is stretched (i.e., the $\tau_{\theta\theta}$ and $\tau_{\phi\phi}$ stress components are negative), and that for a viscoelastic liquid they are given by

$$\tau_{\theta\theta} = \tau_{\phi\phi} = -\left\{\frac{2\mu_0\dot{R}}{R} + \left(\frac{4\mu_0\alpha^2\lambda_1}{1-2\alpha\lambda_1}\right)\left[1 - e^{-(1-2\alpha\lambda_1)(t/\lambda_1)}\right]\right\} \tag{8.11-1}$$

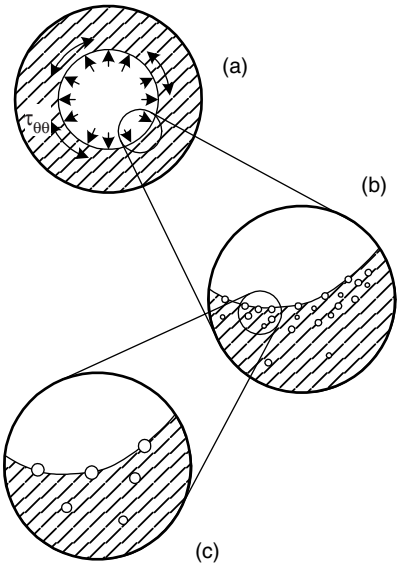

Fig. 8.20 Nucleation mechanism on the surface of a macrobubble. (a) A growing macrobubble generates angular stresses in the surrounding melt; (b) secondary microbubbles nucleate and form blisters; (c) detail of (b).

where μ_0 is the zero shear viscosity, λ_1 is the first relaxation time, and $\alpha = \dot{R}/R$, where R is the macrobubble radius. The order of magnitude of these stresses for a growing bubble was estimated to be (41) 10,000 Pa, as compared to a typical superheat of about 1000 Pa, suggesting a possibly significant role for these cavitation-like stresses on the growing bubble surface in enhancing nucleation rate. Yarin et al. (43) developed a modified nucleation-rate expression accounting for the surface stretching and possible mechanical degradation of the polymer and showed a significantly increasing rate of secondary nucleation with bubble growth.

REFERENCES

1. J. A. Biesenberger, *Devolatilization of Polymers*, Hanser, Munich; also, Macmillan, New York, 1983.
2. R. J. Albalak, Ed., *Polymer Devolatilization*, Marcel Decker, New York, 1996.
3. D. B. Todd, R. H. M. Simon, J. Lane, and J. A. Biesenberger, ''Equipment'' in *Devolatilization of Polymers*, Sec. II, J. A. Biesenberger, Hanser, Munich; Macmillan, New York, 1983.
4. P. S. Mehta, ''An Overview of Devolatilizers,'' in *Polymer Devolatilization*, R. J. Albalak, Ed., Marcel Decker, New York, 1966.
5. R. E. Newman and R. H. S. Simon,''A Mathematical Model for Devolatilization Promoted by Bubble Formation,'' American Institute of Chemical Engineers paper presented at the Annual Meeting, Chicago, 1980.
6. G. A. Latinen, ''Devolatilization of Viscous Polymeric Systems,'' *Adv. Chem. Ser.*, **34**, 235, (1962).
7. R. W. Coughlin and G. P. Canevari, ''Drying Polymers during Screw Extrusion,'' *AIChE J.*, **15**, 560 (1969).
8. G. W. Roberts, ''A Surface Renewal Model for Drying of Polymers during Screw Extrusion'', *AIChE J.*, **16**, 878 (1970).
9. J. A. Biesenberger and G. Kessidis, ''Devolatilization of Polymer Melts in Single Screw Extruders,'' *Polym. Eng. Sci.*, **22**, 832 (1982).
10. P. S. Mehta, L. N. Valsamis, and Z. Tadmor, ''Foam Devolatilization in a Multi-channel Corrotating Disk Processor,'' *Polym. Process. Eng.*, **2**, 103 (1984).
11. A. Tukachinsky, Y. Talmon, and Z. Tadmor ''Foam-enhanced Devolatilization of Polystyrene Melt in a Vented Extruder,'' *AIChE J.*, **40**, 670–675 (1994).
12. P. J. Flory, ''Thermodynamics of High Polymer Solutions,'' *J. Chem. Phys.*, **10**, 51–61 (1942).
13. M. L. Huggins, ''Some Properties of Solutions of Long-chain Compounds,'' *J. Phys. Chem. A.*, **46** (1), 151–158 (1942).
14. J. Brandrup and E. H. Immergut, *Polymer Handbook*, *Third Edition*, Wiley-Interscience, New York, 1989.
15. R. H. M. Simon, ''Flash Evaporators and Falling Strand Devolatilizers'' in *Devolatilization of Polymers*, J. A. Biesenberger, Ed., Hanser, Munich, 1983.
16. D. B. Todd, ''Polymer Devolatilization,'' paper presented at the Society of Plastics Engineers Annual Technical Conference, San Francisco, 1974.

17. J. S. Vrentas and J. L. Duda, *J. Poly. Sci. Part B: Poly. Phys*., **15**, 403 and 417 (1977).
18. H. Fujita, ''Diffusion in Polymer Diluent Systems,'' *Fortschr. Hochpolym. Forsch.*, **3**, 1–47 (1961).
19. J. L. Duda, J. S. Vrentas, S. T. Ju, and H. T. Liu, ''Prediction of Diffusion Coefficients for Polymer Solvent Systems,'' *AIChE J*., **28**, 279 (1982).
20. J. M. Zielinski and J. L. Duda, ''Solvent Diffusion in Polymeric Systems,'' in *Polymer Devolatilization*, R. J. Albalak, Ed., Marcel Decker, New York, 1996.
21. M. Blander and J. L. Katz, ''Bubble Nucleation of Liquids,'' *AIChE J*., **21**, 833 (1975).
22. R. Cole, ''Homogeneous and Heterogeneous Nucleation'' in *Boiling Phenomena*, Vol. 1, S. Van Stralen, and R. Cole, Eds., McGraw-Hill, New York, 1979, Chapter 3.
23. R. T. Knapp, J. W. Daily, and F. G. Hammitt, *Cavitation*, McGraw-Hill, New York, 1970.
24. S. T. Lee and J. A. Biesenberger, ''Fundamental Study of Polymer Melt Devolatilization. IV: Some Theories and Models for Foam-enhanced Devolatilization,'' *Polym. Eng. Sci*., **29**, 782–790 (1989).
25. S. T. Lee, Ph.D. Thesis, Chem. Eng. Dept., Stevens Institute of Technology, Hoboken, NJ.
26. E. N. Harvey, D. K. Barnes, W. D. McElroy, A. H. Whitely, D. C. Pease, and K. W. Cooper, ''Bubble Formation in Animals: I. Physical factors,'' *J. Cellular Comp. Physiol*., **24**, 1 (1944).
27. S. T. Lee, ''A Fundamental Study of Foam Devolatilization'' in *Polymer Devolatilization*, R. J. Albalak, Ed., Marcel Decker, New York, 1996, Chapter 6.
28. C. E. Brennen, *Cavitation and Bubble Dynamics*, Oxford University Press, Oxford, 1995.
29. M. Greenspan, and C. E. Tschiegg, *J. Res. Natl. Bur. Stand. C. Eng. Instrum.*, **71C**, 299–312 (1967).
30. H. B. Marschall, K. A. Mørch, A. P. Keller, and M. Kjeldsen, ''Cavitation Inception by Almost Spherical Particles in Water,'' paper presented at the Fourth International Symposium on Cavitation, California Institute of Technology, Pasadena, CA, June 20–23, 2001.
31. W. L. Wilkinson, ''Entrainment of Air by a Solid Surface Entering a Liquid/Air Interface,'' *Chem. Eng. Sci.*, **30**, 1227 (1975).
32. A. Tukachinsky, Z. Tadmor, and Y. Talmon, ''Ultrasound-enhanced Devolatilization in Polymer Melt,'' *AIChE J*., **39**, 359 (1993).
33. M. Favelukis and R. J. Albalak, ''Fundamentals of Bubble Growth,'' in *Polymer Devolatilization*, R. J. Albalak, Ed., Marcel Decker, New York, 1996.
34. L. E. Scriven, ''On the Dynamics of Phase Growth,'' *Chem. Eng. Sci*., **10**, 1 (1959).
35. E. J. Hinch and A. Acrivos, ''Long Slender Drops in a Simple Shear Flow,'' *J. Fluid Mech.*, **98**, 305 (1980).
36. E. L. Canedo, M. Favelukis, Z. Tadmor, and Y. Talmon, ''An Experimental Study of Bubble Deformation in Viscous Liquids in Simple Shear Flow,'' *AIChE J*., **39**, 553 (1993).
37. M. Favelukis, O. M. Lavrenteva and A. Nir, ''Deformation of a Slender Bubble in a non-Newtonian Liquid in an Extensional Flow,'' *Chem. Eng. Sci.*, **56**, 4643–4648 (2001).
38. M. Favelukis, O. M. Lavrenteva, and A. Nir, ''Deformation an Breakup of a Non-Newtonian Slender Drop in an Extensional Flow,'' *J. Non-Newtonian Fluid Mech*., **125**, 49–59 (2005).

39. M. Favelukis, Z. Tadmor, and Y. Talmon, "Bubble Dissolution in Viscous Liquids in Simple Shear Flow," *J. Non-Newtonian Fluid Mech.*, **41**, 2637–2641 (1995).

40. R. J. Albalak, Z. Tadmor, and Y. Talmon, "Scanning Electron Microscopy Studies of Polymer Devolatilization" *J. Non-Newtonian Fluid Mech.*, **33**, 808–818 (1987).

41. R. J. Albalak, Z. Tadmor, and Y. Talmon, "Polymer Melt Devolatilization Mechanisms," *J. Non-Newtonian Fluid Mech.*, **36**, 1313–1320 (1990).

42. J. R. Street, "The Rheology of Phase Growth in Elastic Liquids," *Trans. Soc. Rheol.*, **12**, 103 (1968).

43. A. L. Yarin, D. Lastochkin, Y. Talmon, and Z. Tadmor "Bubble Nucleation during Devolatilization of Polymer Melts," *AIChE J.*, **45**, 2590–2605 (1999).

PROBLEMS

8.1 ***Equilibrium Concentration of the Solute over the Solution and the Degree of Superheat*** Consider a 5000-ppm styrene–(PS) solution at 200°C ($\chi_{12} = 0.3$ and $P_1^0 = 450$ kPa) placed in a vacuum of 2 mmHg. Assuming identical densities, calculate the maximum final separation possible. What is the degree of superheat?

8.2 ***Determining the Flory–Huggins Interaction Parameter*** χ_{12} Charge a 1-liter vessel with 250 g polymer ($\rho = 1.37$), heat, and evacuate to 1 torr. Add 3.6 mL nitromethane, agitate at 180°C at final pressure of 560 torr. What is χ_{12} for the polymer–nitromethane system?

8.3 ***Staging and Equilibrium*** Methylene chloride (CH_2Cl_2) is to be removed from polymer ($\rho = 1.57$ g/cm^3) containing 8.7% wt CH_2Cl_2 to a residual content of 100 ppm, $\chi_{12} = 0.56$. (a) How many stages should be considered? (b) At 150°C, what is the theoretical vacuum level required in the last stage? (c) Above what temperature should the first stage be maintained to obtain one order of magnitude solvent content reduction, yet keep this stage above atmospheric pressure, in order to avoid fouling large amounts of the devolatilized stream? (d) How much energy (kwh/kg polymer) must be put into the first stage if the feed is at 110°? Assume $C_p = 0.4$ cal/g°C for both solvent and polymer. (e) Calculate the equilibrium pressure and volume of vapor (m^3/kg polymer) removed in each stage when the preceding devolatilizing process is attempted with $n = 1, 2, 3,$ or 4 stages. Assume equilibrium in each stage at 150°C. Use the commonly used assumption $W_j/W_{j+1} = (W_0/W_f)^{1/n}$.

8.4 ***Single Screw Extruder Devolatilization Using Latinen's Model*** Review the paper by Biesenberger and Kessidis* and discuss (a) the experimental method used

*J.A. Biesenberger and G. Kessidis, "Devolatilization of Polymer Melts in Single Screw Extruders," *Polym. Eng. Sci.*, **22**, 832 (1982).

by the authors to verify or disprove the Latinen model; (b) why the Latinen model cannot explain the rate of devolatilization in vacuum-vented screw extruders. (c) Suggest an alternative technique for choosing between a diffusion-controlled and a boiling-type devolatilization mechanism.

8.5 ***The Thermodynamic Pressure–Volume Diagram*** The accompanying figure shows a schematic pressure–volume–temperature diagram for a pure liquid. Trace lines on the diagram showing (a) supersaturation at fixed pressure in terms of temperature difference, and (b) supersaturation at fixed temperature in terms of pressure difference. (c) Explain the meaning of the spinodal line. (d) Explain the difference between the kinetic and thermodynamic limits of superheat.

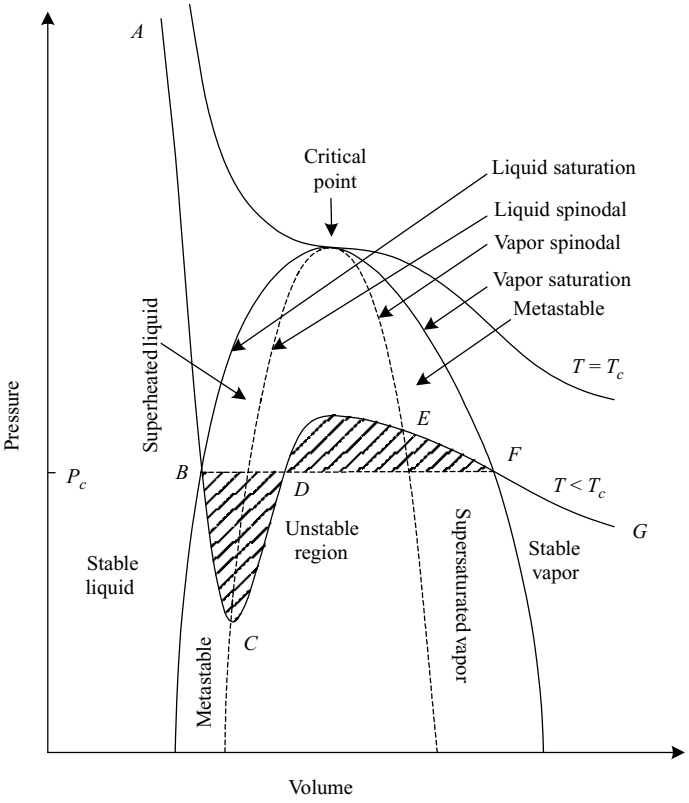

8.6 ***Homogeneous Nucleation*** (a) Using Eq. 8.6-2, calculate the rate of homogeneous nucleation of styrene as a function of temperature at atmospheric pressure and a temperature range from 145°C to 325°C. In calculating the pressure in the bubble, assume that it equals the vapor pressure (extrapolate it from lower temperature values). Use the Eötvös equation $\sigma = 2.1(\rho/M)^{2/3}(T_c - T - 6)$, where the surface tension is in erg/cm^3, temperature is in °C, and density in g/cm^3, to evaluate the surface tension as a function of temperature. The critical temperature

of styrene is 374°C, and the boiling point at atmospheric pressure is 145°C. Homogeneous boiling starts when the rate of nucleation is of the order of 10^6 nuclei per cubic centimeter per second. (b) Explain qualitatively why homogenous nucleation is unlikely in polymer melt devolatilization.

8.7 ***Bubble Growth*** A 1-mm radius bubble with internal pressure of 0.1 atm(g) (above atmospheric pressure) is placed in a polymeric liquid of viscosity 3.5×10^3 Ns/m^2 and surface tension 2.5×10^{-2} N/m at ambient pressure. Calculate the bubble radius as a function of time.

8.8 ***Bubble Deformation*** A 5-mm radius bubble is placed in a viscous liquid of 0.2 $lb_f \cdot s/in^2$ and surface tension of 22 dyne/cm. Calculate the shape of the bubble, the half-length, and slenderness ratio of the bubble at shear rates 1, 10, and 100 s^{-1}.

8.9 ***Affine Deformation of a Liquid Droplet in Simple Shear Flow*** When a drop of liquid is suspended in another liquid undergoing shear or extensional flow, the drop will deform. If the strength of the flow exceeds some critical value, as discussed in the chapter, the drop will break into two or more fragments. In affine deformation the droplet deforms exactly as the surrounding liquid, which implies that the suspended droplet does not disturb the original velocity profile. The accompanying figure shows a two-dimensional drop placed in a simple shear flow $v_x = dx/dt = Gy$ and $v_y = dy/dt = 0$:

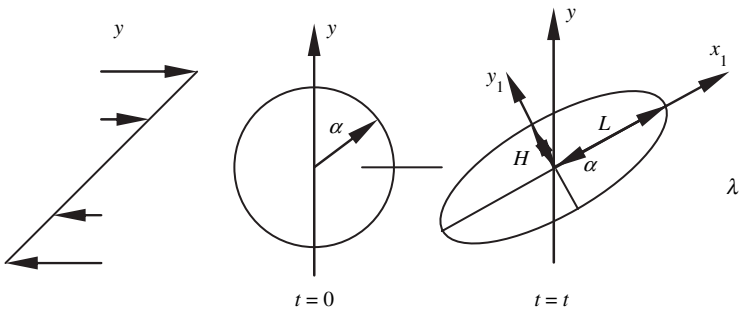

(a) Integrate the velocity profile and show that a point at time $t = 0$ placed at (x_0, y_0) is at time t at position $(x_0 + \tau y, y_0)$, where $\tau = Gt$ is a dimensionless time. (b) At time $t = 0$ a point on the surface of the drop satisfies the equation $x_0^2/a^2 + y_0^2/a^2 = 1$. Show that after time t the shape of the drop is given by $x^2 - 2\tau xy + (1 + \tau^2)y^2 = a^2$. (c) Show that the angle of the major axis of the ellipse with the x-axis is given by $\tan(2\alpha) = 2/\tau$. (d) Show that the shape of the ellipse can be expressed in terms of the of the semimajor L and semiminor H axes as $x_1^2/L^2 + y_1^2/H^2 = 1$.

8.10 ***Affine Deformation of a Liquid Droplet in Extensional Flow*** The shape of a droplet in extensional flow defined by $v_x = dx/dt = Gx$ and $v_y = dy/dt = -Gy$ is shown in the accompanying figure.

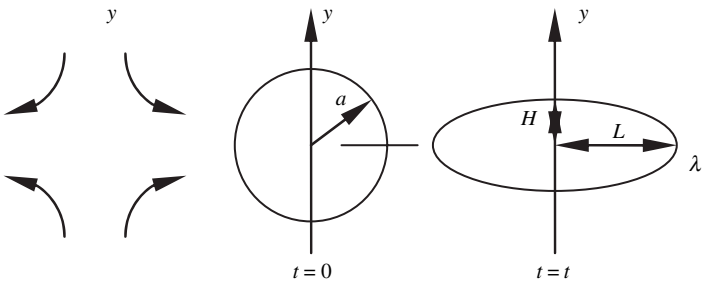

(a) Integrate the velocity profile and show that the original point (x_0, y_0) moves to the position $(x_0 \exp(\tau), y_0 \exp(-\tau))$ at time t, where $\tau = Gt$ is a dimensionless time. (b) Show that the shape of the ellipse is given by $\exp(-2\tau)x^2 + \exp(2\tau)y^2 = a^2$. (c) Show that the semimajor and semiminor axes are given by $L/a = \exp(\tau)$ and $H/a = \exp(-\tau)$.

8.11 ***Devolatilization of Residual Toluene*** Residual toluene is continuously removed from a polymer melt stream of 454 kg/h at 230°C and 0.006 weight fraction of toluene, at a vacuum of 20 torr. The density of the polymer is 0.98 g/cm^3, and the Florry–Huggins interaction parameter is $\chi_{12} = 0.43$. (a) Calculate the equilibrium concentration, w_e. (b) If equilibrium is reached, that is, $w_f = w_e$, where w_f is the final concentration, calculate the separation efficiency $F_S = (w_0 - w_f)/w_0$. (c) If the final concentration $w_f = 2w_e$, calculate F_S. (d) Calculate for (c) the volumetric flow rate of the vacuum pump removing the volatiles.

8.12 ***Elastomer Solution Stagewise Devolatilization*** A stream of 1000 lb/h of an elastomer solution containing 18% wt hexane at 70°F is to be concentrated by heating under pressure and flashing, followed by a two-stage devolatilization to a residual concentration of 0.4% wt. The elastomer must not exceed 320°F to avoid degradation. The flash should not go below 5 psig to make solvent recovery easier and to reduce the potential hazard of air incursion under vacuum. Assume $\chi_{12} = 0.4$, density 1.0 g/cm^3, and that the specific heat of the polymer is the same as for hexane. (a) Estimate the minimum hexane concentration possible under the flash constraints just given. (b) Estimate the process stream temperature following the flash. (c) Calculate the percentage of hexane removed in the flash. (d) Calculate the heat load for the heat exchanger upstream of the flash. (e) Estimate the surface area required. (f) Estimate the first vacuum-stage pressure if operated at 300°F. (g) Calculate the last vacuum-stage pressure, also at 300°F, assuming equilibrium is attained. (h) Calculate the energy loads for the two vacuum stages.

8.13 ***Devolatilizing Screw Extruder*** A 150-mm-diameter, square-pitched, single-flighted screw extruder, with screw channel depth of 25 mm and 20-mm flight width is used to devolatilize a 1000-kg/h stream with 0.78-g/cm^3 density at 200°C and 125 torr. (a) At what frequency of screw rotation will the channel be 30% or less full? (b) With water injection, if density is halved by formation of 1-mm bubbles, how much surface area (per meter length) is created? (c) How does

this surface compare with the available area before and after foaming? (d) Assuming a cubical array of the foam bubbles in the melt, what is the minimum film thickness?

8.14 ***Silo Volatiles Composition*** Polymer flake is fed into a silo at 2820 kg/h containing 0.56% residual cyclohexane. (a) What sweep air rate should be employed to keep the effluent air at less than one-half of the lower explosion limit? (b) Is it permissible from an environmental point of view to release the effluents into the atmosphere?